

New Mexico GEOLOGY

Spring 2021
Volume 43, Number 1



Contents

Late Pennsylvanian Calcareous Paleosols from Central New Mexico: Implications for Paleoclimate

Tanner, Lawrence H. and Lucas, Spencer G. 3–9

New Mexico Graduate Student Abstracts 10–16



Cover

Located about 5 miles northeast of Socorro, the Ojo de Amado is a spring that feeds a pool that is an important source of water for local wildlife. “Ojo” literally means “eye” in Spanish, but the word is used dialectically in New Mexico to refer to a spring. The Ojo de Amado is also known to locals as Bursum Springs, one of several geographic features in the state named after Holm Bursum (1867–1953), a longtime resident of Socorro and an important political figure of the New Mexico Territory who ultimately served in the U. S. Senate from 1921 to 1925. The steeply dipping strata around the Ojo de Amado are Upper Pennsylvanian clastic and carbonate rocks of the Atrasado Formation. They are faulted up just east of the local eastern edge of the Rio Grande rift and along the western flank of the Cerros de Amado, a set of rugged hills developed in Upper Paleozoic strata.

—Photograph by Spencer G. Lucas.

A publication of the
New Mexico Bureau of Geology and Mineral Resources
A Research Division of the
New Mexico Institute of Mining and Technology
Science and Service
ISSN 0196-948X

New Mexico Bureau of Geology and
Mineral Resources
Director and State Geologist
Dr. Nelia W. Dunbar

Geologic Editor: Bruce Allen
Production Editor: Belinda Harrison

EDITORIAL BOARD

Dan Koning, NMBGMR
Barry S. Kues, UNM
Jennifer Lindine, NMHU
Gary S. Morgan, NMMNHS

New Mexico Institute of Mining and Technology
President

Dr. Stephen G. Wells

BOARD OF REGENTS

Ex-Officio

Michelle Lujan Grisham
Governor of New Mexico

Stephanie Rogriguez

Acting Cabinet Secretary of Higher Education

Appointed

Deborah Peacock

President, 2018–2022, Corrales

Jerry Armijo

Secretary-Treasurer, 2015–2026, Socorro

Dr. David Lepre

2021–2026, Placitas

Dr. Yolanda Jones King

2018–2024, Moriarty

Veronica Espinoza, student member

2021–2022, Sunland Park

New Mexico Geology is an online publication available as a free PDF download from the New Mexico Bureau of Geology and Mineral Resources website. Subscribe to receive email notices when each issue is available at geoinfo.nmt.edu/publications/subscribe

Editorial Matter: Articles submitted for publication should follow the guidelines at

geoinfo.nmt.edu/publications/periodicals/nmg/NMGguidelines.html

Address inquiries to Bruce Allen, Geologic Editor, New Mexico Bureau of Geology and Mineral Resources, 801 Leroy Place, Socorro, NM 87801. For telephone inquiries call 575-835-5177 or send an email to NMBG-NMGeology@nmt.edu geoinfo.nmt.edu/publications/periodicals/nmg



Late Pennsylvanian Calcareous Paleosols from Central New Mexico: Implications for Paleoclimate

Spencer G. Lucas, New Mexico Museum of Natural History and Science, Albuquerque, NM 87104, spencer.lucas@state.nm.us
Lawrence H. Tanner, Department of Biological Sciences, Le Moyne College, Syracuse, NY 13214, tannerlh@lemoyne.edu

Abstract

We document calcareous paleosols from Upper Pennsylvanian (lower Virgilian) strata of the Burrego Member of the Atrasado Formation in the Cerros de Amado of Socorro County, New Mexico. The Burrego paleosols are an excellent example of a scarce, climate-sensitive lithology in the Pennsylvanian strata of New Mexico. These paleosols contain mostly stage II to III carbonate horizons, and their overall morphology suggests deposition and pedogenesis under subhumid, seasonally dry conditions. This conclusion is consistent with paleobotanical and other data that indicate such climate conditions were widespread on Late Pennsylvanian Pangea. The mean value of the oxygen-isotope ratios from Burrego paleosol carbonates compares well with the values from Virgilian paleosols of the San Juan, the eastern Midland and Chama basins of New Mexico-Texas, suggesting similar conditions of temperature and paleoprecipitation. Application of the diffusion-reaction model to the mean carbon-isotope composition of the carbonate suggests a paleo- $p\text{CO}_2$ of approximately 400 ppmV, which is also consistent with estimates from correlative carbonate deposits that formed farther east in Late Pennsylvanian Pangea.

Introduction

What have been called “climate-sensitive lithologies” are rock types specific to a particular climate, the best known being coal (wet), gypsum (dry) and calcareous paleosols (seasonally wet/dry). Such rock types play a prominent role in the interpretation of past climates, constrain climate models and are critical to paleogeographic reconstructions (e.g., Boucot et al., 2013; Cao et al., 2019). However, the distribution of climate-sensitive lithologies remains unevenly and incompletely documented, particularly in older geological time periods.

Indeed, in the Pennsylvanian sedimentary rocks of New Mexico, relatively few such rocks have been documented. Thus, coal beds are few and mostly thin, localized and confined to early Middle Pennsylvanian (Atokan) strata (e.g., Armstrong et al., 1979; Kues and Giles, 2004; Krainer and

Lucas, 2013). Gypsum beds are rare, with one well documented example in early Late Pennsylvanian (Missourian) strata (Rejas, 1965; Lucas et al., 2009; Falcon-Lang et al., 2011). Paleosols of Pennsylvanian age, especially climate-sensitive calcareous paleosols, have only been documented from two late Paleozoic basins in northern New Mexico (Tabor et al., 2008; Tanner and Lucas, 2017, 2018). Here, we add to this sparse record of climate-sensitive rocks in the New Mexican Pennsylvanian strata a succession of calcareous paleosols in lower Virgilian strata of Socorro County (Fig. 1).

Stratigraphic context

The calcareous paleosols documented here are in the Burrego Member of the Atrasado Formation, strata that encompass the Missourian-Virgilian boundary, in the Cerros de Amado of Socorro County (Figs. 1-2). Thompson

chronostratigraphy		1. Paradox basin		2. Rowe-Mora basin		3. Orogrande basin				
Permian	Wolfcampian	Cutler Group	Arroyo del Agua Formation	Sangre de Cristo Formation		Abo Formation				
			<div><div></div><div>1</div><div>2</div><div>3</div><div>New Mexico</div></div>	Alamitos Formation	<div><div></div><div>paleosols documented</div></div>	Bursum Formation				
<div><div></div><div>Moya Member</div><div>Del Cuerto Member</div><div>Story Member</div><div>Burrego Member</div><div>Council Spring Member</div></div>	Atrasado Formation					FI				
							<div><div></div><div>Virgilian</div><div>Missourian</div></div>	B	<div><div></div><div></div><div></div></div>	E
			A	C						

Figure 1. Three late Paleozoic basins in New Mexico that have documented calcareous paleosols of Late Pennsylvanian-early Permian age. Relevant publications are A = Tanner and Lucas (2018); B= Tabor et al. (2008); C = Tanner and Lucas (2017); D = Mack (2003) and references cited therein; E = Tabor et al. (2008); F = this paper.

(1942) presented the first detailed lithostratigraphy and biostratigraphy of the Middle-Upper Pennsylvanian strata that crop out in central and southern New Mexico. In this monograph, Thompson (1942) named six formation-rank units in the northern Oscura Mountains of Socorro County that Lucas and Krainer (2009) reduced in rank to members of the Atrasado Formation, including the Burrego Member.

Rejas (1965), in an unpublished master's thesis, brought much of Thompson's (1942) stratigraphic nomenclature

into the Cerros de Amado region east of Socorro (also see Kottlowski, 1960). He used Burrego Member much as did Thompson (1942), as a slope-forming, mixed clastic-carbonate interval between two prominent limestone units, the Council Spring Member (below) and Story Member (above).

Lucas et al. (2009), Barrick et al. (2013) and Krainer et al. (2017) published stratigraphic sections of the Burrego Member and adjacent strata at several locations in the Cerros de Amado and vicinity. However, the

section described here, though very close to one of the sections Lucas et al. (2009) published (their Minas de Chupadera section) was not studied by them. We discovered this section during fieldwork in 2018.

In the Cerros de Amado, the Burrego Member is 13–55 m thick and consists mostly of slope-forming mudstone and shale interbedded with arkosic/micaceous sandstone and limestone (Rejas, 1965; Lucas et al., 2009; Barrick et al., 2013; Krainer et al., 2017). Most limestone beds in the Burrego Member are evidently of marine origin, as they contain marine macrofossils, including algae, crinoids, molluscs and brachiopods. Conodont and fusulinid biostratigraphy indicates the Burrego paleosols are close in age to the Missourian–Virgilian boundary, and we consider them here to be of early Virgilian age (Lucas et al., 2009; Barrick et al., 2013).

Material and methods

We used standard field methods with a 1.5-m staff, tape measure and Brunton pocket transit to measure the thickness of strata in the stratigraphic section discussed here, which is located in the SE ¼ sec. 26, T2S, R1E (UTM coordinates are in the caption to Figure 2), (Fig. 2). Samples were collected for petrographic and isotopic analysis. To confirm the pedogenic origin of the carbonate, standard 30 µm petrographic thin sections were examined for pedogenic fabrics and textures and for evidence of diagenetic effects.

Carbonate aliquots for isotopic analysis were obtained by selectively drilling micritic calcite in lapped slabs corresponding to prepared thin sections with an ultrafine engraving tool while viewing under a binocular microscope. The samples were analyzed for $\delta^{18}\text{O}$ and $\delta^{13}\text{C}$ by the Duke Environmental Stable Isotope Laboratory (Nicholas School of the Environment, Duke University, Durham, North Carolina) using standard operating procedures (see Tanner and Lucas, 2018, for details).

We calculated paleo- pCO_2 using the mean $\delta^{13}\text{C}$ value from 8 samples and the diffusion-reaction model of Cerling (1991, 1999). But, as we did

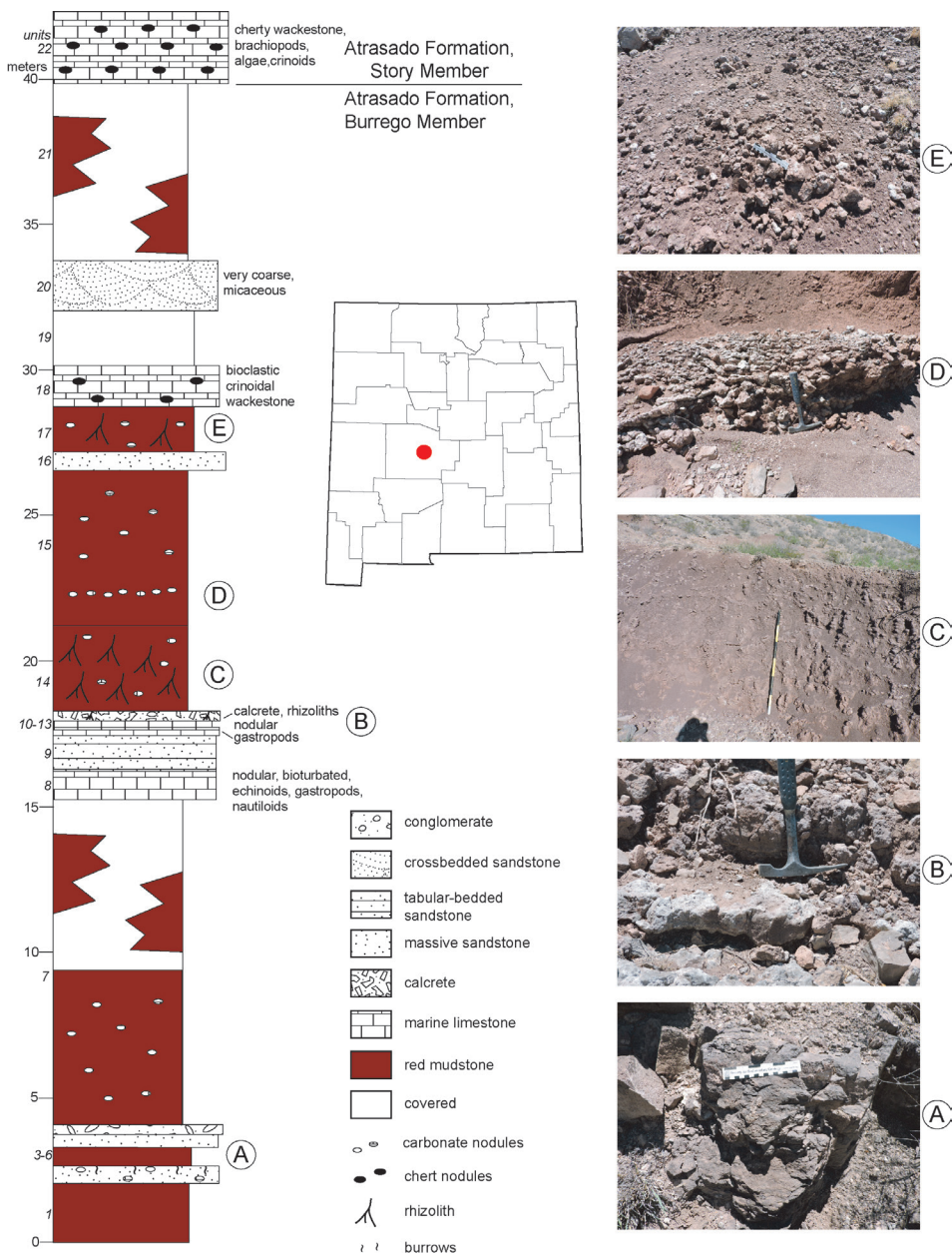


Figure 2. Stratigraphic section of the Burrego Member of the Atrasado Formation near Minas de Chupadera in Socorro County (base of section at UTM 333433, 3775122 and top at 333299, 3775300, zone 13, datum NAD 83; inset map of New Mexico shows location of section in Socorro County). On left, lithostratigraphy of the measured section with the calcareous paleosols in the section labeled A–E. On right, field photographs of the calcareous paleosols A–E.

not obtain organic matter from the samples for determination of $\delta^{13}\text{C}_{\text{org}}$, we applied values from the literature for formations of similar age and geographic proximity (within 2 degrees latitude), primarily from the published data supplements to Montañez et al. (2007, 2016).

Outcrop description

Where the paleosols in the section display sufficiently distinctive pedogenic features to allow classification, we apply the terminology of Mack et al. (1993) in assigning names of paleosol orders, modified by adjectives describing the most prominent subordinate characteristic. The most common paleosol types we found in the measured section are calcic Argillisols and Calcisols to argillic Calcisols. The calcic Argillisol denotes a paleosol horizon in which the defining characteristic is a clay-rich B horizon that is visibly enriched in CaCO_3 in the form of nodules, i.e., a Btk horizon. In any paleosol profile with multiple defining characteristics, such as illuviated clays and pedogenic carbonate, whether they occur in the same horizon or in separate horizons, a subjective judgement was made to determine which feature is dominant and which is subordinate. Thus, there may be a fine distinction between a calcic Argillisol and an argillic Calcisol. In profiles where development of the calcareous B horizons (Bk, or Btk if argillic and calcic) is stronger than the argillic (Bt) horizons, we assign the designation Calcisol or argillic Calcisol, as appropriate. In addition to Argillisols and Calcisols, and variations thereof, we recognize calcic Vertisols, paleosols with prominent vertic fractures and calcareous features in the B horizon. Many mudstone beds of varying thickness display pedogenic features, such as calcareous nodules, drab colors and root traces, but lack distinct horizonation. We term these units Protosols, and where they contain calcareous nodules we label them calcic Protosols. Most paleosol profiles in the section are truncated in that they lack a discernible eluviated upper (A) horizon and display evidence of sediment removal. We also recognize compound profiles in the

section. These are marked by repetition of specific types of B horizons (Bt, Btk or Bk) without an intervening A horizon, suggesting an erosional episode (Kraus and Hasiotis, 2006).

The stratigraphic section we measured encompasses ~ 40 m of most of the Burrego Member and its upper contact with the overlying Story Member (Fig. 2). Most of this stratigraphic section is mudrock, about 82% of the thickness of the strata measured. Minor lithologies are sandstone/conglomerate (11% of the section) and limestone (7% of the section).

The section (Fig. 2) begins with red-bed mudstone overlain by a thin-bedded, ripple-laminated, very-fine grained sandstone that is 0.5 m thick (units 2–3). This sandstone has a platy fabric and contains some discrete calcareous nodules and scarce root traces that increase in abundance upward and has a bioturbated/pedoturbated top. The top 0.1 m is a well-developed carbonate horizon (Stage II of Gile et al., 1966) with carbonate nodules 1 to 2 cm in diameter, drab root traces and rhizoliths up to 5 cm long. We consider unit 2 a truncated Calcisol that is relatively immature, given the lack of coalescing nodules, consisting only of C and Bk horizons. It is overlain by 0.3 m of red mudstone (unit 4) followed by a 0.3-m-thick bed of coarse-grained, arkosic sandstone capped by a 0.1-m-thick limestone-pebble conglomerate (units 5–6). Some of the limestone pebbles in this conglomerate contain marine macrofossils, including brachiopods and gastropods. The overlying unit 7 is 11.3 m thick and is a red mudstone slope with its upper half covered by mostly colluvium. The lower half of this unit has numerous carbonate nodules isolated in the mudstone, but lacks distinct horizonation. Therefore, we consider this unit a calcic Protosol.

Above unit 7 is a nodular and bioturbated limestone (unit 8) rich in marine macrofossils, including echinoids, gastropods and nautiloids. A 1.2-m-thick, very coarse-grained, arkosic sandstone bed (unit 9) above has limestone rip-ups at its base and displays somewhat indistinct, tabular bedding. The overlying interval of limestone (units 10–13) begins with a 0.2-m-thick bed of lime mudstone with

sparse fossils of marine gastropods, capped by a 0.2 to 0.3-m-thick dark to light limestone bed that is nodular, and the weathered surface has vertical channels up to 2.5 cm wide and 10 cm long that are filled with smaller calcareous nodules. We infer that these record root channels formed during subaerial exposure and pedogenesis of the marine carbonate. The top of the unit is a 0.1 m mudstone/limestone breccia consisting of limestone blocks up to 4 cm in a red mudstone matrix with root traces and small calcareous nodules. This unit represents a calcic Argillisol formed on the reworked limestone surface.

Unit 14 is 2.9 m of dark brown, fine-grained mudstone with a crumb fabric, but the outstanding feature of the unit is the presence of numerous rhizoliths. These are calcareous masses that weather out of the outcrop face, mostly vertically oriented and irregular (noncylindrical) in shape. The masses are up to 1.0 m long, 0.1 m in diameter and have no internal structure. Most of these features have a rough, knobby appearance because they consist of vertically stacked, calcareous oblate spheroids of varying diameters. Many of them taper downward, and some exhibit branching, supporting their interpretation as rhizoliths. The unit also contains subhorizontal arcuate soil fractures and irregular (botryoidal) calcareous masses up to 0.1 m wide. Unit 14 lacks any horizonation, so it is interpreted to represent a single B horizon containing calcareous nodules and vertic fractures. We classify this unit as a calcic Vertisol that formed through an extended interval of continuous sedimentation (aggradation) during pedogenesis, in other words, a cumulative paleosol. The outcrop does not contain the top of the unit, and no A-horizon is preserved.

The overlying 5.4 m of red mudstone (unit 15) has clay-lined root traces and numerous carbonate nodules that increase upward to form a coalesced (Stage III to IV) layer 0.6 m thick that is exposed over a lateral extent of 5 m. We regard this unit as the Btk horizon of an argillic Calcisol. The unit is truncated above abruptly by a massive, 0.5-m-thick sandstone ledge (unit 16). The sandstone is overlain by 1.7 m of red mudstone with drab-brown

mottling at the top (unit 17). The mudstone contains numerous rhizoliths and calcareous nodules that increase in abundance vertically to form two horizons, each approximately 0.3 m thick, of carbonate nodules up to 8 cm in diameter, which coalesce to form Stage II to III pedogenic carbonate horizons. Nodules decrease in abundance in the upper 0.4 m of the overlying mudstone interval of unit 17. The transitional nature of the underlying and overlying mudstone intervals of unit 17 suggests that this unit represents a calcareous paleosol, specifically a compound argillic Calcisol with Btk (Stage II) and Bk (Stage III) carbonate horizons.

The overlying bed of limestone (unit 18) is a 1.3 m thick, thickly bedded, cherty bioclastic wackestone with abundant crinoidal debris. Above that is a covered slope 2.1 m thick overlain by a very coarse grained, micaceous, trough crossbedded sandstone (unit 20) that is 1.7 m thick. The uppermost part of the Burrego Member is a 6.1 m thick slope, mostly covered, but where bedrock is exposed on this slope it is red mudstone (unit 21). The base of the overlying Story Member is a medium-bedded, cherty wackestone with fossils of algae, crinoids and brachiopods.

Outcrop interpretation

As noted above, the Burrego Member is a lithosome that includes a mixture of sediments of marine and nonmarine origin, and the section we studied is representative of that. Thus, limestone beds in the section with marine invertebrate fossils (units 8, 12 and 18) are obviously of marine origin, whereas the other strata are of nonmarine origin.

The relatively thick intervals of red mudstone that host the calcareous paleosols we studied are readily interpreted as nonmarine deposits of alluvial floodplains that have undergone variable amounts of pedogenesis. Sandstones in the section are likely of fluvial origin, and limestone clasts in the conglomerate low in the section (unit 6) contain marine invertebrate fossils, which suggests proximity to marine carbonate beds. Thus, we interpret the section as mostly representing floodplain deposition close to the shoreline and sea, interrupted by marine incursions.

The section we studied includes meter-scale profiles of simple and cumulative paleosols, including calcic Argillisols, argillic Calcisols, Calcisols and calcic Vertisols. Most samples for isotopic analysis were selected from

argillic Calcisols and Calcisols with well-developed (Stage III to Stage IV *sensu* Gile et al., 1966; Machette, 1985) carbonate horizons hosted in argillic red beds. Examination of petrographic thin sections indicates that pedogenic carbonate in the section consists of micritic calcite with displacive textures and fabrics, including circumgranular cracking, that demonstrate a lack of diagenetic replacement (Fig. 3). Samples generally were selected from below the coalesced carbonate horizon to maximize depth below the original soil surface.

Paleosol analysis

Four paleosols were sampled for isotopic analysis (labelled A, C, D and E in Figure 2). In ascending order these are: (1) a thin Calcisol with Stage II calcareous paleosol developed in a blocky, very-fine grained sandstone containing calcareous rhizoliths (station A); station B is a nodular carbonate formed on a marine limestone and was not sampled due to the likelihood of incorporation of marine carbonate; (2) station C is a calcic Vertisol exposure, 2.9-m thick, notable for the abundance of calcite-cemented rhizoliths up to 1 meter in vertical length in a mudstone matrix with blocky ped fabric; (3) station D is a Calcisol with a prominent Stage III nodular horizon; and (4) station E is a calcic Argillisol containing two nodular horizons exhibiting Stage II and Stage III morphology, likely representing stages in formation of a cumulative soil.

Petrography reveals the presence of typical alpha-type fabrics in the carbonate nodules sampled in the section, such as grain coronas and corroded floating grains that indicate that these nodules represent the accumulation of carbonate in the B horizon of paleosols (Fig. 3; Alonso-Zarza and Wright, 2010). Thus, we are confident that these carbonates formed within soils developed on alluvial muds.

Isotopic analysis of eight carbonate samples from the Burrego Member are tightly clustered and yielded $\delta^{13}\text{C}_{\text{carb}}$ values ranging from -6.4‰ to -5.6‰ with a mean of $-6.0 \pm 0.1\text{‰}$ (VPDB) (Table 1). The isotopic composition of

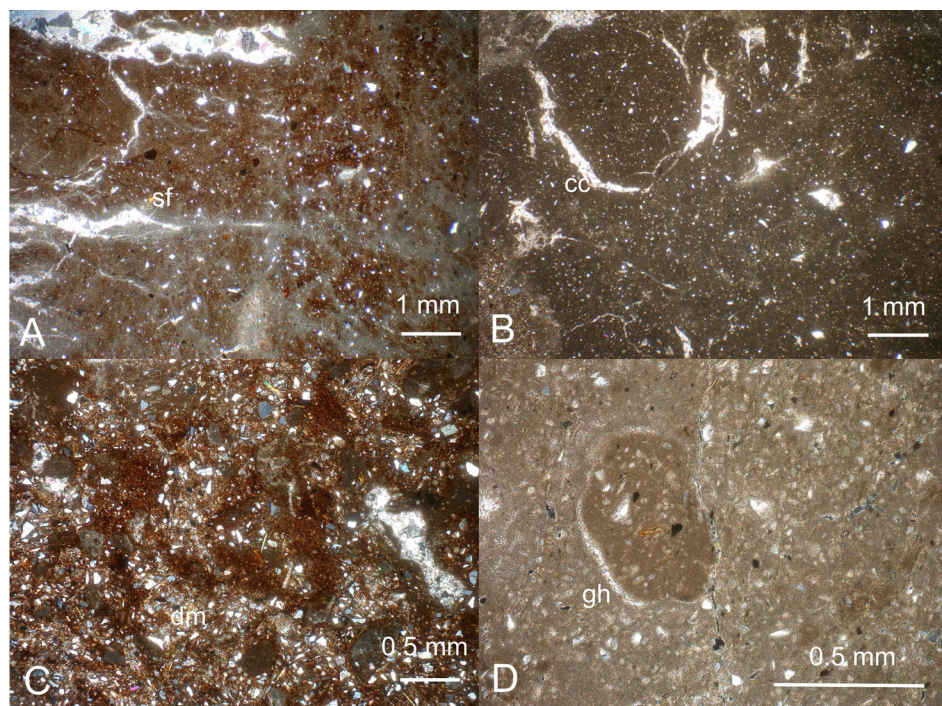


Figure 3. Petrographic features of Burrego Member calcic paleosols. A) Spar-filled voids and shrinkage fractures (sf). B) Mudstone clast surrounded by circumgranular crack (cc). C) Mudstone matrix with displacive micrite (dm). D) Mudstone clast surrounded by sparry grain halo (gh).

two samples from rhizoliths at Station C (-6.0 ‰, -5.6 ‰ (VPDB)) is the same as measured in samples of carbonate nodules, suggesting micritization of the root casts in the deep (>50 cm depth) soil environment and therefore representative of the isotopic composition of soil respired CO₂. Values of δ¹⁸O have a wider spread, ranging from -5.7 to -1.8 ‰, with a mean value of -3.4 ± 0.5 ‰ (VPDB). The greater range for δ¹⁸O likely records pedogenic carbonate precipitation under a range of temperature and/or precipitation conditions. The composition of the carbonate is determined by a combination of factors in the diffusion model: plant respiration rate, isotopic composition of the plant organic matter (OM), atmospheric isotope composition and pCO₂. The isotopic composition of the plant OM tells us about the vegetation, but only in the most general sense (C3 vs C4), and nothing is known about any possibly unique isotopic aspects of Pennsylvanian plant OM.

The lack of δ¹³C_{om} measurements in this study makes application of the diffusion-reaction model of Cerling (1991; 1999) somewhat problematic. However, the datasets of Montañez et al. (2007, 2016) provide useful measurements of δ¹³C_{om} that allow us to at least make an approximation of paleo-pCO₂. Temperature of soil carbonate formation, the isotopic composition of atmospheric CO₂ and the contribution of soil-respired CO₂ (the S(z) term) are also required for application of the model. We assumed values based on (but not identical to) those of Montañez et al. (2007, 2016), using values δ¹³C_{om} = -21.0 ‰, δ¹³C_a = -2.5 ‰ (composition of atmospheric CO₂), T = 25°C and S(z) = 3000 ppmV. The S(z) value reflects the fact that carbonate precipitation mainly occurs during the drier months when plant productivity is decreased (Breecker, 2013). The Burrego carbonates yielded a mean δ¹³C_{carb} of -6.0 ‰. Using the values cited above we obtained a paleo-pCO₂ for the early Virgilian of ~400 ppmV. This estimate accords well with values presented by Montañez et al. (2016) for the late Missourian, and the early Virgilian (Fig. 4). The mean δ¹⁸O value of -3.4 ± 0.5 ‰ (VPDB) obtained compares well with the values

from the Virgilian paleosols of the Chama Basin of northern New Mexico (Tanner and Lucas, 2018), suggesting similar conditions of temperature and paleoprecipitation.

Overall, the morphology of the paleosols in the Burrego Member suggests deposition and pedogenesis under subhumid, seasonally dry conditions. The calcareous paleosol horizons vary in maturity from Stage II to IV, and both cumulate and composite paleosol profiles are present, suggesting higher rates of sedimentation during some intervals, alternating with slow sedimentation during others (e.g., Deutz et al., 2002; Monger et al., 2009). In particular, the “mega-rhizolith” horizon at Station C appears to be a single, undifferentiated B horizon with an exposed thickness of 2.9 m. This attests to continuous aggradation of the surface contemporaneous with pedogenic processes, particularly rooturbation. The interplay of sedimentation and biological activity with pedogenesis suggests meteoric precipitation at the higher end of the range for which calcareous paleosol formation is considered possible (Birkeland, 1999; Retallack,

2005). Thus, paleosol morphology supports the isotopic analyses in suggesting sediment deposition and soil formation under widely varying moisture conditions.

Table 1. Isotopic analyses of Burrego calcareous paleosol samples. Values in units ‰ VPDB.

Unit	δ ¹⁸ O	δ ¹³ C
Station A	-3.8	-5.8
Station C-1	-3.5	-5.6
Station C-2	-4.0	-6.0
Station D-1	-2.6	-6.2
Station D-2A	-4.0	-6.1
Station D-2B	-5.7	-6.4
Station E-1	-1.8	5.9
Station E-2	-2.1	-5.6

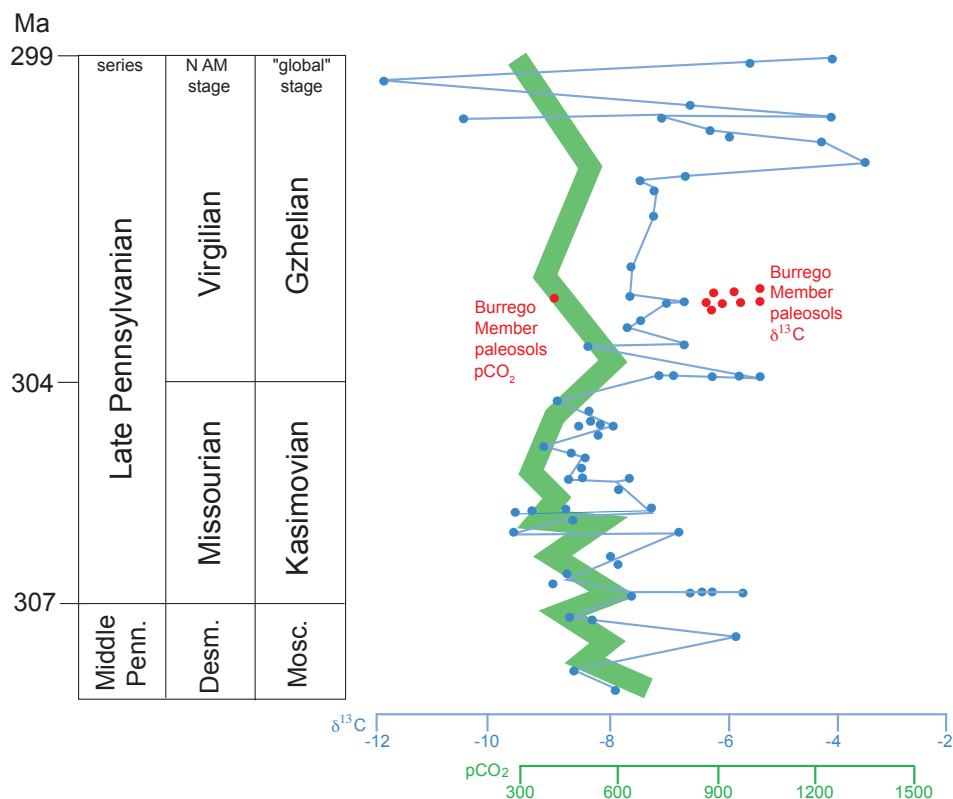


Figure 4. Compilation of Late Pennsylvanian δ¹³C_{carb} data from Montañez et al. (2016), the pCO₂ curve of Chen et al. (2018) calculated from the Montañez et al. data, δ¹³C_{carb} values obtained in this study, and the calculated pCO₂ value from the Burrego Member.

Discussion

In New Mexico, sedimentary rocks of late Paleozoic age are synorogenic deposits of the Ancestral Rocky Mountain (ARM) orogeny. Driven by the Gondwana–Laurussia collision that amalgamated late Paleozoic–Mesozoic Pangea (e. g., Kluth and Coney, 1981; Dickinson and Lawton, 2003), the ARM in New Mexico produced a series of basement-cored uplifts surrounded by sedimentary basins during Middle Pennsylvanian (Atokan)-early Permian (Wolfcampian) time (e.g., Kues and Giles, 2004; Brotherton et al., 2020). The result was an archipelago of islands (the uplifts) surrounded by shallow-marine sedimentary basins during the Middle–Late Pennsylvanian, followed by mostly nonmarine deposition in these and reconfigured sedimentary basins during the early Permian culmination of the ARM orogeny. Around the fringes and on the flanks of the uplifts, nonmarine fluvial deposition took place in some locations during the Pennsylvanian, such as the section described here, and by early Permian time fluvial deposits (largely siliciclastic red beds) were filling the formerly marine basins.

Calcareous paleosols are comparatively common in lower Permian strata in New Mexico (particularly in the Abo Formation: Mack, 2003 and references cited therein), but a few Virgilian calcareous paleosols are the only Pennsylvanian examples that have been documented prior to the Burrego Member record documented here. Thus, Tabor et al. (2008) briefly discussed a few late Virgilian calcareous paleosols in the Rowe–Mora basin (Taos trough) and in the Bursum Formation of southern New Mexico, and Tanner and Lucas (2018) documented similar late Virgilian paleosols in part of the Paradox basin (Fig. 1). These workers concluded that the Virgilian paleosols indicate highly variable climate ranging from subhumid to semiarid with extremes in seasonal precipitation, which is consistent with our interpretation of the Burrego paleosols.

New Mexico was located near the western end of the Pangean tropical belt during the Late Pennsylvanian.

Climate models, paleosol data and paleobotany converge to identify a distinct monsoonal pattern of moisture in western Pangea during the Late Pennsylvanian–early Permian, with moisture sourced from Panthalassa (e.g., Parrish, 1993; Tabor and Montañez, 2004; Tabor and Poulsen, 2008). There was a global shift from wetter Middle Pennsylvanian climates to drier Late Pennsylvanian climates that began in New Mexico during the Middle Pennsylvanian (Desmoinesian) when floras with seasonally dry elements begin to appear and then become more common during the Late Pennsylvanian and early Permian (DiMichele et al., 2011, 2017).

In central New Mexico, the Atrasado Formation, including the Burrego Member, contains a succession of paleofloras that are all of “mixed” composition. This means that plants that favored wet substrates and those from habitats with seasonal moisture limitations are mixed together in the fossil assemblages and evidently grew in close proximity. These floras indicate climates that varied from subhumid to semiarid and arid (DiMichele et al., 2017).

The Burrego paleosols formed in a subhumid climate under seasonally dry conditions. The $p\text{CO}_2$ value of ~ 400 ppm we calculate is within the range of values given by Montañez et al. (2016, fig. 2) across the Missourian–Virgilian boundary. Thus, the Burrego paleosols indicate a climate within the range of what were thought to be the climates of equatorial Pangea during the Late Pennsylvanian—subhumid and seasonally dry. The Burrego paleosols thus add an important data point of climate sensitive lithologies from what was far western, tropical Pangea during the Late Pennsylvanian.

Acknowledgments

The comments of the reviewers, D. O. Breecker and H. C. Monger, and the editor, B. D. Allen, improved the content and clarity of the manuscript.

References

- Alonso-Zarza, A.M. and Wright, V.P., 2010b, Calcretes; *in* Alonso-Zarza, A.M. and Tanner, L.H., eds., Carbonates in Continental Environments: Processes, Facies and Applications: Developments in Sedimentology 61: Elsevier, Amsterdam, p. 226–267.
- Armstrong, A.K., Kottowski, F.E., Stewart, W.J., Mamet, B.L., Baltz, E.H., Jr., Siemers, W.T. and Thompson, S., III, 1979. The Mississippian and Pennsylvanian (Carboniferous) systems in the United States—New Mexico. U. S. Geological Survey, Professional Paper 1110-W, p. W1–W27.
- Barrick, J., Lucas, S. G., and Krainer, K., 2013, Conodonts of the Atrasado Formation (uppermost Middle to Upper Pennsylvanian), Cerros de Amado region, central New Mexico, USA: New Mexico Museum of Natural History and Science, Bulletin 59, p. 239–252.
- Birkeland, P.W., 1999, Soils and Geomorphology, 3rd ed., Oxford, New York, 536 pp.
- Boucot, A.J., Chen, X., Scotese, C.R. and Morley, R.J., 2013, Phanerozoic paleoclimate: an atlas of lithologic indicators of climate: SEPM Concepts in Sedimentology and Paleontology, no. 11, Map Folio, 28 maps.
- Breecker, D.O., 2013, Quantifying and understanding the uncertainty of atmospheric CO_2 concentrations determined from calcic paleosols: Geochemistry, Geophysics, Geosystems, v. 14, p. 3210–3220.
- Brotherton, J.L., Chowdhury, N.U.M.K., and Sweet, D.E., 2020, Synthesis of late Paleozoic sedimentation in central and eastern New Mexico: Implications for timing of ancestral Rocky Mountains deformation: SEPM Special Publication 113. doi: 10.1021/sepmsp.113.03.
- Cao, W., Williams, S., Flament, M., Sahirovic, S., Scotese, C. and Müller, R.D., 2019, Palaeolatitudinal distribution of lithologic indicators of climate in a palaeogeographic framework: Geological Magazine, v. 156, p. 331–354.
- Cerling, T.E., 1991, Carbon dioxide in the atmosphere: evidence from Cenozoic and Mesozoic paleosols: American Journal of Science, v. 291, p. 377–400.
- Cerling, T.E., 1999, Stable carbon isotopes in paleosol carbonates; *in* Thiry, M. and Simon-Coinçon, R., eds., Palaeoweathering, palaeosurfaces and related continental deposits: International Association of Sedimentologists, Special Publication 27, p. 43–60.
- Chen, J., Montañez, I.P., Qi, Y., Shen, S., and Wang, X., 2018, Strontium and carbon isotopic evidence for decoupling of $p\text{CO}_2$ from continental weathering at the apex of the late Paleozoic glaciation: Geology, v. 46, p. 395–398.

- Deutz, P., Montañez, I.P. and Monger, H.C., 2002, Morphology and stable and radiogenic isotope composition of pedogenic carbonates in late Quaternary relict soils, New Mexico, USA: an integrated record of pedogenic overprinting: *Journal of Sedimentary Research*, v. 72, p.809–822.
- Dickinson, W.R., and Lawton, T.F., 2003, Sequential intercontinental suturing as the ultimate control of Pennsylvanian Ancestral Rocky Mountains deformation: *Geology*, v. 31, p. 609–612.
- DiMichele, W.D., Cecil, C.B., Chaney, D.S., Elrick, S.D., Lucas, S.G., Lupia, R., Nelson, W.J. and Tabor, N.J., 2011, Pennsylvanian-Permian vegetational changes in tropical Euramerica; *in* Harper, J.A., ed., *Geology of the Pennsylvanian-Permian in the Dunkard basin: 76th Annual Field Conference of Pennsylvania Geologists Guidebook*, Washington, PA, p. 60–102.
- DiMichele, W.A., Chaney, D.S., Lucas, S.G., Nelson, W.J., Elrick, S.D., Falcon-Lang, H.J. and Kerp, H., 2017, Middle and Late Pennsylvanian fossil floras from Socorro County, New Mexico, U.S.A: *New Mexico Museum of Natural History and Science, Bulletin* 77, p. 25–99.
- Falcon-Lang, H.J., Jud, N.A., Nelson, W.J., DiMichele, W.A., Chaney, D.S. and Lucas, S.G., 2011, Pennsylvanian coniferopsid forests in sabkha facies reveal the nature of seasonal tropical biome: *Geology*, v. 39, p. 371–374.
- Gile, L.H., Peterson, F.F., and Grossman, R.B., 1966, Morphological and genetic sequences of accumulation in desert soils: *Soil Science*, v. 100, p. 347–360.
- Kluth, C.F. and Coney, P.J., 1981, Plate tectonics of the Ancestral Rocky Mountains: *Geology*, v. 9, p. 10–15.
- Kottlowski, F.E., 1960, Summary of Pennsylvanian sections in southwestern New Mexico and southeastern Arizona: *New Mexico Bureau of Mines and Mineral Resources, Bulletin* 66, 187 p.
- Krainer, K., and Lucas, S.G., 2013, The Pennsylvanian Sandia Formation in northern and central New Mexico: *New Mexico Museum of Natural History and Science, Bulletin* 59, p. 77–100.
- Krainer, K., Vachard, D., Lucas S.G., and Ernst, A., 2017, Microfacies and sedimentary petrography of Pennsylvanian limestones and sandstones of the Cerros de Amado Area, east of Socorro (New Mexico, USA): *New Mexico Museum of Natural History and Science, Bulletin* 77, p. 159–198.
- Kraus, M.J. and Hasiotis, S.T., 2006, Significance of different modes of rhizolith preservation to interpreting paleoenvironmental and paleo-hydrologic settings: examples from Paleogene paleosols, Bighorn Basin, Wyoming, U.S.A.: *Journal of Sedimentary Research*, v. 76, p. 633–646.
- Kues B.S., and Giles K.A., 2004, The late Paleozoic Ancestral Rocky Mountains system in New Mexico; *in* Mack G.H., and Giles, K.A., eds., *The Geology of New Mexico, A Geologic History: New Mexico Geological Society, Special Publication* 11, p. 95–136.
- Lucas, S.G. and Krainer, K., 2009, Pennsylvanian stratigraphy in the northern Oscura Mountains, Socorro County, New Mexico: *New Mexico Geological Society, Guidebook* 60, p. 153–166.
- Lucas, S.G., Krainer, K., and Barrick, J.E., 2009, Pennsylvanian stratigraphy and conodont biostratigraphy in the Cerros de Amado, Socorro County, New Mexico: *New Mexico Geological Society, Guidebook* 60, p. 183–212.
- Machette, M.N., 1985, Calcic soils of the southwestern United States: *Geological Society of America, Special Paper* 203, p. 1–21.
- Mack, G.H., 2003, Lower Permian terrestrial palaeoclimate indicators in New Mexico and their comparison to palaeoclimate models: *New Mexico Geological Society, Guidebook* 54, p. 231–240.
- Mack, G.H., James, W.C., and Monger, H.C., 1993, Classification of paleosols: *Geological Society of America Bulletin*, v. 105, p. 129–136.
- Monger, H.C., Cole, D.R., Buck, B.J. and Gallegos, R.A., 2009, Scale and the isotopic record of C4 plants in pedogenic carbonate: from the biome to the rhizosphere: *Ecology*, v. 90, p.1498–1511.
- Montañez, I.P., Tabor, N.J., Niemeier, D., DiMichele, W.A., Frank, T.D., Fielding, C.R., and Isbell, J.L., 2007, CO₂-forced climate and vegetation instability during late Paleozoic deglaciation: *Science*, v. 315, p. 87–91.
- Montañez, I.P., McElwain, J.C., Poulsen, C.J., White, J.D., DiMichele, W.A., Wilson, J.P., Griggs, G., and Hren, M.T., 2016, Climate pCO₂ and terrestrial carbon cycle linkages during Late Palaeozoic glacial-interglacial cycles: *Nature Geoscience*, v. 9, p. 824–831.
- Parrish, J.T., 1993, Climate of the supercontinent Pangaea: *Journal of Geology*, v. 101, p. 215–33.
- Rejas, A., 1965, Geology of the Cerros de Amado area, Socorro County, New Mexico: [M.S. thesis]: *New Mexico Institute of Mining and Technology, Socorro*, 128 p.
- Retallack, G.J., 2005, Pedogenic carbonate proxies for amount and seasonality of precipitation in paleosols: *Geology*, v. 33, p. 333–336.
- Tabor, N.J., and Montañez, I.P., 2004, Permo-Pennsylvanian alluvial paleosols (north-central Texas): High-resolution proxy records of the evolution of early Pangean paleoclimate: *Sedimentology*, v. 51, p. 851–884.
- Tabor, N.J. and Poulsen, C.J., 2008, Palaeoclimate across the Late Pennsylvanian–early Permian tropical palaeolatitudes: a review of climate indicators, their distribution, and relation to palaeophysiographic climate factors: *Palaeogeography, Palaeoclimatology, Palaeoecology*, v. 268, p. 293–310.
- Tabor, N.J., Montañez, I.P., Scotese, C.R., Poulsen, C.J. and Mack, G.H., 2008, Paleosol archives of environmental and climatic history in paleotropical western Pangea during the latest Pennsylvanian through Early Permian: *Geological Society of America, Special Paper* 441, p. 291–303.
- Tanner, L.H., and Lucas, S.G., 2017, Paleosols of the Upper Paleozoic Sangre de Cristo Formation, north-central New Mexico: Record of early Permian palaeoclimate in tropical Pangea: *Journal of Palaeogeography*, v. 6, p. 144–162.
- Tanner, L.H., and Lucas, S.G., 2018, Pedogenic record of climate change across the Pennsylvanian–Permian boundary in red-bed strata of the Cutler Group, northern New Mexico, USA: *Sedimentary Geology*, v. 373, p. 98–110.
- Thompson, M.L., 1942, Pennsylvanian System in New Mexico: *New Mexico School of Mines, State Bureau of Mines and Mineral Resources, Bulletin* 17, 92 p.

New Mexico Graduate Student Abstracts

New Mexico Geology recognizes the important research of graduate students working in M.S. and Ph.D. programs. The following abstracts are from M.S. theses and Ph.D. dissertations completed in the last 12 months that pertain to the geology of New Mexico and neighboring states.

New Mexico Institute of Mining and Technology

TWO-STAGE LANDSLIDE EMBLACEMENT ON THE ALLUVIAL APRON OF AN EOCENE STRATOVOLCANO

Chirigos, Michael G., M.S.

The Sawtooth Mountains, western New Mexico, comprise erosionally isolated klippen of an initially contiguous landslide complex that developed on the alluvial apron of an Eocene stratovolcano during late Laramide volcanic-tectonic activity. Volcanogenic siltstone, alluvial sandstone and conglomerate of the lower Spears Group were deposited on mainly fine-grained Baca Formation (fluvial flood-plain facies). The klippen are underlain by a locally exposed, low-angle fault within fine-grained, laminated basal Spears strata (distal fan). The lower fault is overlain by a sheet 7–100 m thick of sandy volcanogenic sandstone (Volcaniclastic Unit of Largo Creek, mid-fan facies) that is strongly deformed by large-scale soft-sediment structures. Another low-angle fault caps this sheet, and carries less-deformed conglomerates (Dog Springs Formation, proximal fan facies).

The lower fault, where exposed, has a poorly developed fault core, locally comprised of floury or foliated gouge, and surrounded by a thin, poorly developed fractured damage zone. The upper fault has a well-developed cataclastic core, 0.12–0.40 m thick, with 1–3 primary slip surfaces, rare pseudotachylyte, and local cataclastic injections into the upper plate. Striations on both faults are widely dispersed but cluster in two directions, NNE and ESE. The main structure in the upper plate is an E-vergent monocline.

We conclude that the landslide complex was emplaced in two events, first N-directed sliding down the alluvial apron, while the sediments were poorly consolidated. Most soft-sediment deformation probably occurred in this event, due to loading and shear transmitted down from the upper plate, causing liquefaction. The second event was likely due to W-side-up uplift on the Laramide Hickman Fault, located west of the field area, likely was triggered by an earthquake, and occurred at seismogenic slip rates, forming pseudotachylyte on the upper detachment and injections, after the sediments were partially lithified.

CHEMOSTRATIGRAPHY OF THE BONE SPRING FORMATION, DELAWARE BASIN, SE NEW MEXICO.

Foli, Isaac David, M.S.

The Bone Spring Formation is a middle Permian mixed carbonate and clastic turbidite petroleum reservoir in the Delaware Basin of west Texas and southern New Mexico. It consists of

shelf to basin sandy turbidites and carbonate mass-transport deposits sourced from the north and northeastern shelf margins during Leonardian time (275 Ma). Compositional heterogeneity within this unit is poorly understood but strongly impacts the spatial and temporal distribution of reservoir forming elements. Substantial research has focused on the Bone Spring Formation, but little work has been undertaken to understand the depositional controls on intramember mineralogy and compositional heterogeneity of the formation within a chemostratigraphic framework. The aim of our research is to characterize the bulk geochemical and lithologic heterogeneity within the Bone Spring Formation to better understand the depositional controls effecting stratigraphic hierarchy.

Element data is presented from 837 feet (255 meters) of Bone Spring Formation core from Eddy and Lea county of New Mexico and identify compositional changes at the foot scale. Bulk element data collected via handheld XRF analyses conducted at an unbiased 6 inch spacing in the cores. XRF bulk composition was analyzed statistically using principal component analysis (PCA) and hierarchical cluster (HCA) analysis to determine stratigraphic heterogeneity from a chemofacies standpoint. Distinct changes in mineralogy describe chemostratigraphic units that relate to depositional trends and the evolution of Delaware Basin stratigraphy in the Leonardian.

Understanding the compositional heterogeneity of the Bone Spring Formation has implications for petroleum system analysis in the Delaware Basin and overlying hydrocarbon reservoirs such as the Brushy Canyon Formation. Our results help to define mechanical properties intrinsic to the compositional architecture of the Bone Spring Formation and will help to improve future well development in the Delaware Basin. Furthermore, our work demonstrates the suitability of handheld XRF as a tool to quickly generate and assess large geochemical datasets to describe stratigraphic changes in deep-water deposits and in their relation to sequence stratigraphic evolution.

CARBONATE-WHITE PHYLLOSILICATE ALTERATION OF INTRUSIVE ROCK IN THE NORTHERN KELLY MINING DISTRICT, NEW MEXICO

Herman, Colton Tate, M.S.

The polymetallic Kelly mining district is located in the northern Magdalena Mountains, Socorro County, New Mexico approximately 170 kilometers south-southwest of Albuquerque. Mineralization mainly occurs as manto-like carbonate replacement deposits (CRD) and locally minor skarn, both of which primarily replaced Mississippian-age limestone. Hardscrabble Valley, located in the northern extent of the district, contains the Tertiary-age (28 Ma) intrusion known

as the Nitt Monzonite. The Nitt Monzonite is pervasively potassically and phyllically altered with local late-stage vein-controlled propylitic alteration assemblages. Carbonate-phyllic alteration observed in the Nitt Monzonite consists of sericite + carbonate + quartz + chlorite ± pyrite. This alteration style is atypical of the classic quartz-sericite-pyrite (QSP) type phyllic alteration of porphyry copper deposits.

The Nitt Monzonite exhibits an inherently low permeability (<<1% volume), yet hydrothermal fluid has pervasively permeated and altered this intrusion. Petrographic observations imply that mineral replacement reactions from the interaction of a hydrothermal fluid produced net-zero to negative volume changes in the Nitt Monzonite. This creation of space during mineral-fluid reactions facilitated the infiltration of the hydrothermal fluid through the Nitt Monzonite, resulting in the precipitation of secondary quartz in voids as phyllic alteration was developed and evolved in this hydrothermal system.

Electron microprobe data shows secondary phengites are of an intermediate composition, known as aluminocladonite, with a range of $(K_{0.69-0.96}Na_{0.02-0.26}Ca_{0.03})Al_{1.64-1.94}Mg_{0.02-0.25}Fe^{2+}_{0.0-0.18}(Si_{3.08-3.41}Al_{0.59-0.92})O_{10}(OH_{1.88-1.96}F_{0.0-0.12})$. Secondary chlorite is Mg dominant, representing a clinoclinal end-member species, with a range of $(Mg_{4.936-26}Fe^{2+}_{3.19-3.92}Mn_{0.12-0.37}Ti_{0.0-0.02}Al_{2.14-2.64})(Si_{5.51-6.06}Al_{1.94-2.49})O_{20}(O_{16}H_{15.61-15.85}F_{0.11-0.26})$. Calcite is the exclusive carbonate mineral in the phyllic alteration assemblage.

Microthermometric analyses of primary fluid inclusions in secondary quartz associated with the phyllic alteration styles indicate the trapping of a high-density fluid during quartz deposition. Homogenization temperatures range from 172–427°C; with an average of 296°C. Halite-bearing fluid inclusions are common within this secondary quartz and the measured salinities range from 43–54 wt.% NaCl equivalent, implying that some of the trapped fluid was hypersaline. Primary liquid-dominant and vapor-dominant fluid inclusions are locally present within some individual hydrothermal quartz crystals, suggesting the trapping of a boiling fluid occurred in quartz, at least locally, during the history of the phyllic alteration.

Short-wave infrared spectroscopic analyses (SWIR) performed on phyllically altered samples show Al-OH absorption wavelengths between 2198–2214 nm with an average of 2209 nm, consistent with other studies reporting aluminocladonite. Shorter average Al-OH wavelengths (2203–2205 nm) of samples in the south-central area of Hardscrabble Valley are characteristic of a more muscovitic composition, which may imply proximity to the hydrothermal fluid source.

The geologic features of Hardscrabble Valley are inferred to have formed as a result of

initial development of a graben associated with collapse of the Magdalena caldera during the mid-Tertiary. This study infers that, although not exposed at present erosion levels, a magma intruded the fault zone associated with the graben and generated a magmatic hydrothermal fluid which interacted with indigenous carbonate strata in the subsurface. The dissolution of carbonate resulted in modification of the magmatic fluid which rose to upper structural levels and reacted with the Nitt Monzonite, producing the carbonate phyllic alteration. This process may be related to underlying calcsilicate alteration in the subsurface rock units, with the potential for accompanying base metal mineralization.

QUANTIFYING THE TIMESCALES OF ERUPTIONS AND RESURGENCE FOLLOWING CALDERA COLLAPSE: $^{40}\text{Ar}/^{39}\text{Ar}$ DATING AND VOLUME ESTIMATIONS OF POST-CALDERA VOLCANISM AT VALLES CALDERA, NORTHERN NEW MEXICO
Nasholds, Morgan Wade Maynard, Ph.D.

Despite recognition as one of the greatest volcanic hazards in the southwestern United States, many aspects of the post-caldera history of Valles caldera are poorly constrained. This study provides 49 new high-precision $^{40}\text{Ar}/^{39}\text{Ar}$ sanidine ages and surface volume estimations to reveal insights into lifespans of dome emplacement as well as resurgence. Caldera collapse and deposition of the Tshirege Member of the Bandelier Tuff at 1231.6 ± 1.0 ka was followed by emplacement of 34 volcanic units erupted from vents on the resurgent dome and along the caldera-ring fracture. New ages indicate vent and dome complexes that followed collapse were emplaced during polygenetic and monogenetic eruptive events. The Deer Canyon rhyolite eruptions began immediately following caldera formation and lasted until 1220.5 ± 3.6 ka for a total lifespan of 11.4 ka. Similarly, the Redondo Creek Member erupted between 1199.0 ± 5.9 ka and 1186.3 ± 2.9 ka for a lifespan of 12.7 ka. Cerro del Medio, the oldest post-resurgent dome, is also the longest-lived ring-fracture complex, erupting seven units in 25.2 ka between 1157.2 ± 3.1 and 1132.0 ± 4.7 ka. Following Cerro del Medio, Cerros del Abrigo erupted at least twice between 1009.8 ± 1.7 and 997.0 ± 1.6 ka. These longer-lived dome complexes are located within structurally-complex zones of the caldera suggesting the dense network of faults promote magma transport to the surface, producing long-lived eruptions. Conversely, the six dome and vent complexes that erupted between 804.7 ± 1.9 ka and 68.7 ± 1.0 ka have shorter eruptive lifespans than the early post-caldera eruptions. Three of the complexes—San Antonio Mountain, South Mountain, and the East Fork Member—are polygenetic with lifespans between 5.2 and 5.5 ka. The Cerro Santa Rosa 2, Cerro San Luis, and Cerro Seco domes are either monogenetic or polygenetic with lifespans less than the associated age uncertainties. The mapped post-caldera units are grouped into a total of 15 eruptive events, bracketed by measurable intra- and inter-dome repose periods. Combined with the total duration of dome and vent lifespans

of 81.9 ka, the calculated intra-dome eruptive frequency is 1 eruption event per 5.5 ka for when Valles caldera enters periods of sustained dome emplacement. Volume estimations, along with published volumes of the youngest eruptions, indicate that the post-caldera dome and vent complexes range in volume from 0.8 km^3 to 14.1 km^3 and have both increased and decreased throughout post-caldera evolution. In contrast, eruptive flux following caldera collapse has systematically increased between each post-caldera volcanic complex from 0.09 to $2.56 \text{ km}^3/\text{ka}$ during post-caldera evolution. Using new ages of the caldera-forming ignimbrite, a syn-resurgent lava, and the oldest post-resurgent ring-fracture eruption, the resurgence durations at Valles caldera are constrained to be between 74.4 ± 3.3 ka and 41.8 ± 6.7 ka. The average magmatic flux during resurgence is between 0.52 and $0.92 \text{ km}^3/\text{ka}$, which is similar to pluton-filling rates, suggesting that resurgence is partially explained by a significant decrease in magmatic flux following the large fluxes that sustain caldera-forming magma bodies. Establishing an accurate timing of rapid events during post-caldera evolution is possible due to the combination of dating only sanidine grains without melt inclusion-hosted excess ^{40}Ar and the ability of ARGUS VI mass spectrometer to identify problematic grains that skew the weighted mean ages. The eruptive frequency during dome activity and increasing flux has important implications should Valles caldera enter a new phase of volcanic activity. Likewise, developing similar comprehensive age and volume datasets is necessary to assess hazards at other Quaternary volcanic systems.

IMPLICATIONS OF CRYPTIC, NONSTOICHIOMETRIC URANIUM MINERALIZATION ON THE FORMATION AND LEACHABILITY OF SANDSTONE-HOSTED URANIUM ORES, GRANTS DISTRICT, NEW MEXICO

Pearce, Alexandra Rose, Ph.D.

This dissertation consists of three studies examining sandstone-hosted uranium ores from the Grants uranium district in northwestern New Mexico. The first investigates the mineralogy of primary-type uranium ores from the Jackpile Sandstone and Brushy Basin members of the Jurassic Morrison Formation. These ores are characterized by cryptic mineral and mineraloid mixtures, and uranium hosted by “uraniferous organic matter.” The host organic matter and the uranium mineralization is interpreted as having been fixed within the sediments during multistage groundwater mixing episodes involving one or more brines and humic acid-bearing fluid(s) that resulted in humate flocculation. The second study evaluates the environmental geochemistry of ores of the Jackpile Sandstone sampled from the St. Anthony Mine in Cibola County, NM. The site, slated for remediation, was assessed by its responsible party using a geochemical model which used the uranyl silicate mineral uranophane to determine alternate abatement standards for uranium in groundwater. In our examination, we did not find uranophane. Batch leaching tests showed that significant uranium,

vanadium and arsenic are released under oxidizing, alkaline conditions. Groundwater leaching experiments showed appreciable release of uranium and vanadium, but not arsenic. The third study investigates the leachability of redistributed-type ores from the Westwater Canyon Member, and primary-type ores of the Jackpile Sandstone and Brushy Basin members. Here, leaching tests using alkaline lixiviants and ambient groundwater showed that gangue mineralogy and the non-mineral hosts of uranium produce leaching trends entirely discordant to those of stoichiometric minerals previously identified as important components in these deposits (meta-tyuyamunite, meta-autunite, uraninite).

RAINFALL-RUNOFF RELATIONSHIPS IN THE ARROYO DE LOS PINOS, SOCORRO, NEW MEXICO

Richards, Madeline A., Ph.D.

The Arroyo de los Pinos is an ephemeral tributary to the Rio Grande located in central New Mexico, draining an area of 32 km^2 . In 2018 the US Bureau of Reclamation funded a sediment transport study at the confluence of the arroyo and the Rio Grande, with the goal of monitoring sediment influx to the mainstream channel in order to better inform sediment transport models. To supplement this study and to enable generalization to other ephemeral tributaries, more information was needed on up-basin flow generating processes. This thesis focuses on these efforts to characterize the runoff generating mechanisms.

A network of eighteen pressure transducers and five rain gauges were installed throughout the arroyo's watershed in various subbasin tributaries. Pressure transducers monitored water stage data, and these were converted to discharge hydrographs for each flow event. The runoff events monitored this way were all small, close to the threshold of runoff generation, and did not fully activate the channel network. Tipping bucket rain gauges monitored rainfall. Data collected from this network show that rainfall intensity, subbasin lithology and antecedent soil moisture conditions are the primary factors that control runoff initiation, while total rainfall depth and lithology are the main controls on runoff ratio, and subbasin area is the main control on lag time.

Prior to transducer installation, a particularly large flood on 7/26/2018 left behind high-water marks at several locations throughout the watershed. These high-watermarks were surveyed and used as a proxy for maximum flood stage at each location. Peak stage comparisons show that maximum infiltration occurs in the lower third of the watershed that is dominated by alluvial cover and where the channel develops a multi-threaded planform. Results from a relative gravity survey conducted in 2018 confirm that maximum infiltration occurs in the lower elevations of the watershed, where the channel is multi-threaded and flows over alluvium.

PENNSYLVANIAN-PERMIAN EVOLUTION OF THE DARWIN BASIN OF EASTERN CALIFORNIA: BASIN DEVELOPMENT IN THE BACK-ARC OF THE INCIPIENT CORDILLERAN SUBDUCTION ZONE. *Vaughn, Lochlan Wright, Ph.D.*

The Pennsylvanian-Permian Darwin Basin of Eastern California records the abrupt onset of large-magnitude subsidence of the southwestern margin of Laurentia. The basin formed in the late Pennsylvanian but continuously expanded during the early Permian as subsidence and extensional faulting allowed calciclastic base-of-slope apron depositional systems to retrograde on to the subsided slope and shelf. Areal expansion of the Darwin Basin propagated east and southeast through time and is marked by the first deposition of deep-water facies in areas that had been carbonate shelves since the Ordovician. A nearly identical stratigraphic and structural evolution is present in the Pennsylvanian-Permian of southern California, indicating that the driver of subsidence in the Darwin Basin was able to affect a large swath of the southwestern margin of Laurentia at once. Furthermore, subsidence in the Pennsylvanian-Permian of California coincides with a significant change in deformation style of Ancestral Rocky Mountains basins and uplifts, suggesting that the driver of subsidence in California may have affected tectonics across southwestern Laurentia. Speculative basin evolution models invoke tectonism associated with the Late Paleozoic continent-truncating California-Coahuila transform fault as the principal driver of subsidence in the Darwin Basin and southern California. However, the onset of large-magnitude subsidence in southern and eastern California is spatially and temporally associated with the first appearance of magmatism and volcanoclastic sedimentation in the Late Paleozoic of the southwestern U.S. The geochemistry of these early to middle Permian igneous rocks, which include plutons and lavas in southern California and newly identified tuffs in eastern California, demonstrates that these rocks formed in a continental subduction zone. The presence of continental arc-derived igneous rocks in the early Permian of California is interpreted to indicate that the onset of Cordilleran Subduction occurred earlier than has previously been recognized.

We present 15 new measured sections, facies analysis, clast and point counts, and new conodont biostratigraphy that document the Pennsylvanian-Permian evolution of the Darwin Basin. We also report on whole-rock geochemistry and XRD analysis of five previously unknown tuffs identified in the Darwin Basin. We propose that subsidence in the Darwin Basin and southern California was caused by extension and dynamic topography above the incipient Cordilleran Subduction Zone. We further suggest that the first appearance of this subsidence dates the onset of subduction, which appears to have begun shortly before the Pennsylvanian-Permian boundary. Arc magmatism may have begun as early as 290 Ma, but was likely low-volume and confined to small portions of the southwestern plate margin during the Permian, as is the case for the nascent Neo-

gene and Quaternary Puysegur Subduction Zone of New Zealand. The formation of a subduction zone on the southwestern margin of Laurentia would end the transmission of transpressional stress from the California-Coahuila Transform Fault that drove Ancestral Rocky Mountains uplift. Our timeline for the onset of Cordilleran Subduction is independently supported by detailed studies of ARM basins which indicate that the slip on high-angle faults that drove ARM uplift ended at the Pennsylvanian-Permian boundary.

New Mexico State University

PROVENANCE AND SEDIMENT MIXING TRENDS OF THE PLIO-PLEISTOCENE ANCESTRAL RIO GRANDE FLUVIAL SYSTEM, RIO GRANDE RIFT, NEW MEXICO *Parker Ridl, Shay, M.S.*

Pliocene-Pleistocene strata that record axial-fluvial sedimentation of the ancestral Rio Grande fluvial system crop out in New Mexico and southern Colorado, and they preserve the history of drainage evolution and late-stage exhumation of the Rio Grande rift. Presented here are new U-Pb detrital zircon data (N=8 samples; n=2382 analyses) from the Camp Rice and Palomas formations collected at two to three stratigraphic intervals in the Socorro, Hatch-Rincon, Jornada del Muerto, and Mesilla basins. U-Pb ages were then integrated with similar, previous studies from age-equivalent strata that are exposed in southern Colorado and northern New Mexico to develop sedimentary mixing models for the entire Rio Grande rift corridor in this region.

New U-Pb detrital zircon data from the central and southern portion of the Rio Grande fluvial system record peak ages at 34, 167, 519, 1442, and 1686 Ma, suggesting that the ancestral Rio Grande was receiving detritus from late Cenozoic volcanic fields (e.g., San Juan and Mogollon Datil volcanic fields), recycled Mesozoic stratigraphy (Mesozoic eolianites), and Proterozoic basement provinces (e.g., A-Type granitoids and the Mazatzal and Yavapai provinces). Although peak ages across the southern Rio Grande rift are similar across all basins and stratigraphic horizons in this study, there are distinct spatial and temporal, up-section changes in provenance recorded across the southern Rio Grande fluvial system in central and southern New Mexico. Basal strata (~5.0–4.5 Ma) record the largest contributions of detritus derived from the San Juan and Mogollon Datil volcanic fields (34–29 Ma) and lesser occurrences of recycled Cordilleran arc zircons derived from recycled Mesozoic stratigraphy from the Colorado Plateau. The late Pliocene phase (3.1–2.6 Ma) marks similar contributions of detritus derived from late Cenozoic volcanic fields and marks the emergence of peaks that overlap with recycled Cordilleran arc sources (217–82 Ma). Pleistocene (2.0–1.6 Ma) stratigraphic horizons show a relative decrease of zircons that overlap in age with the San Juan and Mogollon Datil volcanic field sources and an increase in contributions of recycled Cordilleran

arc zircons (92–223 Ma). Isolated, secondary Cambrian peak ages occur at the 2.0 Ma stratigraphic horizon in the Mesilla basin and 3.1 Ma stratigraphic horizon in the Socorro basin and overlap in age with Cambrian intrusions that have been reported from parts of New Mexico and southern Colorado (519–516 Ma). All stratigraphic horizons record contributions derived from Precambrian basement sources that were being exhumed during Oligocene-Miocene rifting.

Mixing models were determined from the Rio Grande rift corridor in southern Colorado and throughout New Mexico and used with detrital zircon provenance trends to better understand the timing and nature of drainage development. Inputs for mixing models required grouping source areas into three primary provinces that included detritus from (1) late Cenozoic volcanic fields primarily associated with the San Juan and Mogollon Datil volcanic fields, (2) recycled Mesozoic strata (reflecting previously determined Mesozoic eolianite provenance signatures); and (3) recycled Paleozoic and Precambrian basement that crop out along the Rio Grande rift flanks.

The earliest phase of drainage development (~5.0–4.5 Ma) in northern New Mexico was characterized by elevated detrital contributions from recycled Mesozoic stratigraphy likely derived from the Colorado Plateau, whereas basins in central and southern New Mexico were receiving detritus largely from rift flanks (i.e., Paleozoic and Precambrian sources) and late Cenozoic volcanic-field sources. The late Pliocene (3.1–2.6 Ma) phase of drainage development in northern New Mexico was marked by a relative decrease in detrital contributions from recycled Mesozoic strata. The model shows nearly equal detrital contributions from recycled Mesozoic strata, rift flank, and volcanic field sources at the 3.1–2.6 Ma stratigraphic horizon in central and southern New Mexico. The Pleistocene (2.0–1.6 Ma) phase of drainage development records a shift in provenance in the southern rift basins and models suggest decreased contributions from late Cenozoic volcanic field and rift flank sources, and increased contributions from recycled Mesozoic stratigraphy.

Provenance data and mixing trends that demonstrate increased detrital contributions from recycled Mesozoic strata of the Colorado Plateau support a model of headward erosion of the Rio Puerco into the Jemez Lineament and southwestern margin of the Colorado Plateau during the Plio-Pleistocene. Headward erosion and possibly minor exhumation along the western margin of the rift resulted in increased detrital contributions from the oldest and deepest parts of caldera sources between the Pliocene and late Pliocene. These same caldera source areas were less of a source for the system by the Pleistocene.

ERUPTIVE VOLUME AND EXPLOSION ENERGY ESTIMATES FROM KILBOURNE HOLE MAAR, SOUTH-CENTRAL NEW MEXICO *Vitarelli, Daniela C., M.S*

Maar-diatremes are a common type of monogenetic volcano defined by ascending magma

interacting explosively with an external water source, or phreatomagmatic activity. In terms of area, Kilbourne Hole is an unusually large and irregularly shaped, young (~20 ka) maar with well exposed and accessible deposits. Traditional field methods and complementary remote sensing methods were used to investigate the potential eruptive volume, explosion energy, and eruption progression of Kilbourne Hole maar to shed light on large maar-forming eruptions. With a minimum total eruptive volume of 0.23 km³, Kilbourne is the largest known single maar by eruptive volume. The deposits around the maar crater rim range in thickness from ~1 to ≥60 m. The thickness of individual beds also varies, with beds generally increasing in thickness towards the north-northeast particularly up-section, suggesting vent migration potentially occurred at Kilbourne or that the vent was located northward towards the later stages of the eruption. The deposits themselves lack a later magmatic phase and are dominated by fine ash and sand-waves, indicating emplacement largely by dilute density currents (surges), suggesting that the water-magma ratio remained constant throughout the eruption and that explosions occurred dominantly at greater-than-optimal scaled depths (OSD), which produce abundant surges. The total explosion energy predicted by crater dimensions ranges from 5.21×10^{16} to 1.45×10^{17} J, which when compared to the explosion energies derived from individual events, suggests a range of 54 to 209 explosions of 6.94×10^{14} J would be required to form Kilbourne Hole maar. Although the individual explosion energies predicted at Kilbourne are not necessarily more energetic than those predicted by previous maar studies, the thick deposits and large eruptive volume suggest a prolonged eruption is likely responsible for the large maar-forming eruption and that in some special circumstances, maar eruptions dominated by greater-than-OSD explosions may produce large volumes. While further work is needed to investigate the lateral changes in the deposits at Kilbourne, particularly in the west, and further assess the potential for vent migration at this location, this study has demonstrated that prolonged activity, consistent water-magma ratios, and greater-than-OSD dominated explosions can result in large maar-forming eruptions and result in immense eruptive volumes.

University of New Mexico

NEOGENE DRAINAGE REVERSAL AND COLORADO PLATEAU UPLIFT IN THE SALT RIVER AREA

Anderson, Jordan Curtis, M.S.

The modern Salt River flows southwest from the Colorado Plateau, through the Arizona Transition Zone and into the Basin and Range. Rivers in this area flowed northeast during the Paleogene from the Laramide Mogollon Highlands into structural basins of the topographically lower southern Colorado Plateau area. One of these rivers carved the Salt River paleocanyon through a portion of the Mogollon Highlands known as the Apache Uplift to similar depths as the mod-

ern Grand Canyon. This study refines the timing of this drainage reversal in the Salt River area by constraining the ages of paleoriver sediments deposited during the time of northeast-flowing rivers, internal drainage and southwest-flowing rivers. These results provide insights into the evolution of the southern Colorado Plateau.

U-Pb dating of detrital zircon is used for maximum depositional ages and provenance analyses. ⁴⁰Ar/³⁹Ar dating of detrital sanidine is used for higher precision maximum depositional ages. The majority of paleoriver samples that were analyzed with both detrital zircon and sanidine show similar maximum depositional ages. Minimum or direct depositional ages are determined by overlying or interbedded volcanic units.

The Mogollon Rim Formation is composed of river gravel, sandstone and mudstone on the southern rim of the Colorado Plateau that were deposited by northeast-flowing rivers. Results indicate deposition began after 59.38 Ma in the Flying V Canyon area and from 37–33.55 Ma in the Trout Creek section. The Whitetail Conglomerate represents the transition from northeast-flowing rivers to internal drainage in the Salt River paleocanyon. Whitetail Conglomerate is as old as the interbedded 37.6 Ma dacite in Canyon Creek fault side drainages, but deposition in the axis of the Salt River paleocanyon occurred between 30 and 21.8 Ma. The transition from northeast-flowing rivers to internal drainage occurred between 33.55–30 Ma, marking the age of initial development of the southern edge of the Colorado Plateau. Apache Leap tuff flowed NE down the Salt River paleocanyon nearly to Canyon Creek fault at 18.6 Ma. Internal drainage is documented by the 14.67 Ma Black Mesa basalt that flowed onto underlying lake beds. The first southwest-flowing river system in the Salt River paleocanyon deposited the Dagger Canyon conglomerate after incising at least 200 m deep into the Whitetail Conglomerate. The lower Dagger Canyon conglomerate is present in tilted fault blocks on the eastern side of Tonto Basin and the western portion of the Salt River paleocanyon. The dip of bedding increases down-section from 0 to 27° providing evidence that deposition occurred while the faults were active. Lower Dagger Canyon conglomerate deposition began after 12.49 Ma, presumably due to base level fall associated with Basin and Range extension. The upper Dagger Canyon conglomerate is composed of flat-lying river gravels and sandstone located at higher elevations than the lower Dagger Canyon conglomerate in Tonto Basin and the Salt River paleocanyon. Deposition of the upper Dagger Canyon conglomerate began after 7.34 Ma and a possible lag in fluvial deposition occurred between the two facies. If a lag in fluvial deposition occurred then the upper Dagger Canyon conglomerate represents a rejuvenation of the southwest-flowing river system in the Salt River paleocanyon after Basin and Range faulting waned. A likely driver for this rejuvenation would be southern Colorado Plateau uplift by the building of Mount Baldy volcanic field 12–8 Ma.

FLUVIAL GEOMORPHIC AND HYDROLOGIC EVOLUTION AND CLIMATE CHANGE RESILIENCE IN YOUNG VOLCANIC LANDSCAPES: RHYOLITE PLATEAU AND LAMAR VALLEY, YELLOWSTONE NATIONAL PARK

Burnett, Benjamin Newell, Ph.D.

Quaternary volcanism associated with the last caldera cycle in Yellowstone National Park included emplacement of ash-flow tuffs, massive rhyolite flows ranging from 79 to 484 ka, and valley-filling basalts. This study examines (1) the evolution of spring hydrology with flow age on the Rhyolite Plateau, (2) initial development and evolution of stream networks on the rhyolite flows, and (3) the impact of the 630 ka caldera formation and volcanic flow emplacement on Lamar Valley incision rates.

Integrated stream networks formed within 79 kyr on the Rhyolite Plateau. Incision is focused on steep flow margins and knickpoints and is dependent on local stream power. Plugging of fractures causes hydraulic conductivity of the flows to decline over time. Snowmelt infiltrates rapidly into younger flows, leaving ephemeral surface streams, but many flow-margin springs experience a delayed snowmelt response and enhanced discharge during late-summer periods of water stress, providing important refugia for aquatic organisms threatened by climate change. Incision rates over the past 630 kyr in the Lamar Valley are greatest (≤ 0.55 mm/yr) where the greatest thickness of Quaternary volcanic material was emplaced, where they are higher than most rivers in the region. Incision rates are lowest (≤ 0.15 mm/yr) above a knickpoint caused by erosion resistant crystalline bedrock, and in the upper reaches of two tributaries, where I infer that faulting associated with caldera formation led to stream capture of portions of the headwater areas.

BASAL TRAVERTINE OF THE BOUSE FORMATION: GEOCHEMISTRY, DIAGENESIS AND IMPLICATIONS FOR THE INTEGRATION OF THE COLORADO RIVER

Ferguson, Christina, M.S.

The Pliocene Bouse Formation is discontinuously exposed in the lower Colorado River region and is a record of the first arrival of the Colorado River to the Gulf of California 5 million years ago. It consists broadly of a lower carbonate member (travertine, marl, and bioclastic units) and an upper siliciclastic member (claystone, mudstone, and Colorado River sands). This paper focuses on the basal travertine (synonymous with “tufa”) unit of the lower carbonate member. Because of its basal position and its chemical encrustation of pre-Bouse topography, the travertine can offer insight into the earliest depositional settings and may be a proxy for the composition of the waters that deposited the first Bouse carbonates. Hence the travertine unit, if it can be shown to preserve a primary geochemical signal, offers the potential to discriminate between alternative hypotheses for marine versus non-marine deposition of the Bouse carbonates of the Blythe Basin. This paper examines the geochemistry of the travertine unit

using stable isotopes of carbon and oxygen, $^{87}\text{Sr}/^{86}\text{Sr}$, petrographic examinations of thin sections, and microprobe traverses. Testing for diagenesis included subsampling techniques and textural studies using thin section examinations and SEM investigations.

The travertine unit forms an encrustation that drapes and mantles pre-Bouse topography, including volcanic bedrock and fanglomerates. The travertine unit is generally thin, often less than several meters thick although it can reach thicknesses of tens of meters. It is intermittent but fairly widespread in the Blythe Basin, the southernmost of the Bouse basins, and also is present in scattered locations in the more northern basins. Its facies include: porous tufa, microbialite domes (bioherms), vegetation-casts (charophytes of marsh and probable non-marine origin), and botryoidal travertine, all overlapped by and interfingered with marl and high energy bedforms of bioclastic sandstone that were deposited before the first arriving Colorado River sands. This Walther's Law relationship suggests that the travertines are broadly coeval with the other facies in the basal carbonate unit of the Bouse Formation. Stable isotope data for travertine reveal a covariation of $\delta^{13}\text{C}$ with $\delta^{18}\text{O}$ and a spread of values between (+4, +2‰) and (-16, -9‰) for the southern Blythe Basin and a regression line with $R^2 = 0.63$. Northern basin travertines have a similar covariation trend ($R^2 = 0.73$). Travertines show multiple carbonate generations in thin section, but stable isotope analyses did not show continuous or regular differences in composition of subsamples. Silica diagenesis was observed in the Buzzard's Peak area where the 4.834 Ma Lawlor Peak tuff is interbedded with carbonates, but this area showed overlapping carbonate chemistry to other areas, although somewhat more positive along the regression line. Compiled and new $^{87}\text{Sr}/^{86}\text{Sr}$ analyses show that the basal Bouse carbonates have non-marine values of ~ 0.711 (as opposed to 0.709 for seawater) in all carbonate facies (marls, bioclastic unit, travertine, and numerous fossil types). Double dissolution tests for $^{87}\text{Sr}/^{86}\text{Sr}$ values were performed in travertine and marl to evaluate potential diagenetic changes: these revealed little change in values (from 0.71051 to 0.71081; from 0.71056 to 0.71074; and from 0.71088 to 0.71088). Plots of $\delta^{18}\text{O}$ versus $^{87}\text{Sr}/^{86}\text{Sr}$ and versus latitude show no covariation in $^{87}\text{Sr}/^{86}\text{Sr}$ over a wide range of $\delta^{18}\text{O}$ and facies types.

The combined data are interpreted as showing only limited carbonate diagenesis within the basal travertine of the Bouse Formation such that carbonate geochemistry can be used as a proxy for the waters that deposited them. Two possibilities are examined to explain the covariation of $\delta^{18}\text{O}$ with $\delta^{13}\text{C}$: 1) mixing of sea water (0, 0) and meteoric water (-16, -7); or 2) evaporation of basin water. We favor evaporation as the dominant explanation based on the similarity of travertine variation in northern (lacustrine) and southern (debated marine versus lacustrine) basins, the presence of non-marine charophytes in travertines, and absence of covariation between $\delta^{18}\text{O}$ and $^{87}\text{Sr}/^{86}\text{Sr}$, consistent with evaporation but not mixing. Radiogenic $^{87}\text{Sr}/^{86}\text{Sr}$ and the presence of localized zones of large volumes of

travertine suggest influences from deeply circulated geothermal groundwaters. We do not rule out mixing of marine and non-marine waters in an estuarine environment to explain marine fossils and reported sequence stratigraphic and tidal sedimentary evidence, but the geochemical data are more consistent with the interpretation that the initial travertine deposition in multiple Bouse basins (and the travertine depositing waters) were dominantly non-marine.

INTERPRETING AMALGAMATION PROCESSES OF A FLUVIAL SANDSTONE OF THE NACIMIENTO FORMATION IN THE SAN JUAN BASIN, NEW MEXICO *Miltenberger, Keely Elizabeth, M.S.*

Outcrop studies of fluvial sand bodies are important for the study of fluid transport and storage capabilities because the deposits are heterogeneous. 3-D photogrammetry was used to evaluate the amalgamation processes of a multi-storey sheet sandstone in the San Juan Basin, NM. The Angel Peak Member was deposited in the proximal-medial transition of a distributive fluvial system by a meandering river during the Paleocene. Within the study area, amalgamation occurred by avulsion and reoccupation of channel-belts to produce five storeys of the multi-storey sheet sandstone. Within each storey is evidence of processes that are internal to a channel-belt, such as bar migrations, small scour surfaces, and chute deposits. Vertical truncation by subsequent channel-belts has occurred to each storey. Miocene to present erosion has also removed portions of the uppermost storeys within the detailed study area. The multi-storey sheet sandstone of the Angel Peak Member was deposited as the San Juan Basin was almost full, thus has many characteristics of amalgamation during low accommodation space.

INTEGRATED STUDIES OF INTRACONTINENTAL DEFORMATION IN THE INTERIOR WESTERN USA, CRETACEOUS TO RECENT

Thacker, Jacob Oliver, Ph.D.

The advent of plate tectonic theory satisfactorily explained a number of deformation belts around the world. However intracontinental deformation (deformation inboard of a plate margin) remains poorly understood in plate tectonic models. In order to further our understanding of intracontinental tectonics and its effects, this dissertation examines paleotectonic and neotectonic settings within the interior western USA.

Chapter 1 focuses on late Miocene–Recent deformation inboard of the San Andreas plate margin fault and its role on the integration history of the lower Colorado River. The neotectonic analysis included geometric and kinematic fault data collected in key geologic units to characterize the timing and style of deformation in an area that has commonly been considered to lack young deformation. It is found that post-12 Ma deformation in the region is cumulatively significant and persisted before, during, and after deposition of the Bouse Formation—a unit that represents the first arrival of the Colorado River—

in a (possibly active) zone of inboard transtension.

The remaining chapters focus on Late Cretaceous and younger tectonism within the Laramide foreland region, a world class study area that is still vigorously debated after over 100 years. Chapter 2 utilizes apatite thermochronology to address the timing of Cretaceous (Laramide) and Miocene–Recent tectonism recorded in distinctly situated samples within the Zuni Mountains of west-central New Mexico. Chapter 3, through integrated apatite thermochronology and basin stratigraphy, interprets a ca. 95–70 Ma eastward sweep of Laramide onset of deformation (when it began) across northern Arizona–New Mexico. Chapter 4 scales up the methodology of Chapter 3 with a regional scale compilation effort to interpret an east-northeast directed sweep of time transgressive onset of Laramide deformation from Montana–South Dakota to Arizona–New Mexico during the Late Cretaceous–Paleogene.

These studies contribute to our understanding of plate tectonics and the role that intracontinental deformation plays. Inboard plate margin deformation and its role on river system integration and potential ongoing deformation are described. Likewise, the timing and spatio-temporal patterns of deformation shed light on the tectonic processes that operated during the Laramide orogeny, as well as additional Cenozoic exhumation related to epeirogenic uplift of the western and southwestern United States.

LANDSCAPE EVOLUTION OF THE SOUTHERN COLORADO PLATEAU USING LOW-TEMPERATURE APATITE THERMOCRONOLOGY AND DETRITAL ZIRCON AND SANIDINE PROVENANCE STUDIES *Winn, Carmen L., Ph.D.*

Chapter 1: Westernmost Grand Canyon
Conflicting hypotheses about the timing of carving of the Grand Canyon involve either a 70 Ma (“old”) or < 6 Ma (“young”) Grand Canyon. This paper evaluates the controversial westernmost segment of the Grand Canyon where the following lines of published evidence firmly favor a “young” Canyon. 1) North-derived Paleocene Hindu Fanglomerate was deposited across the present track of the westernmost Grand Canyon, which therefore was not present at ~ 55 Ma. 2) The 19 Ma Separation Point basalt is stranded between high relief side canyons feeding the main stem of the Colorado River and was emplaced before these tributaries and the main canyon were incised. 3) Geomorphic constraints indicate that relief generation in tributaries and on plateaus adjacent to the westernmost Grand Canyon took place after 17 Ma. 4) The late Miocene–Pliocene Muddy Creek Formation constraint shows that no river carrying far-traveled materials exited at the mouth of the Grand Canyon until after 6 Ma. Interpretations of previously-published low-temperature thermochronologic data conflict with these lines of evidence, but are reconciled in this paper via the integration of three methods of analyses on the same sample: apatite (U-Th)/He ages (AHe), $^4\text{He}/^3\text{He}$ thermochronometry ($^4\text{He}/^3\text{He}$), and apatite fission-track ages and lengths (AFT). “HeFTy” software was used

to generate time-temperature (t-T) paths that predict all new and published $^4\text{He}/^3\text{He}$, AHe, and AFT data to within assumed uncertainties. These t-T paths show cooling from $\sim 100^\circ\text{C}$ to $40\text{--}60^\circ\text{C}$ in the Laramide (70–50 Ma), long-term residence at $40\text{--}60^\circ\text{C}$ in the mid-Tertiary (50–10 Ma), and cooling to near-surface temperatures after 10 Ma, and thus support a “young” westernmost Grand Canyon.

A subset of AHe data, when interpreted alone (i.e., without $^4\text{He}/^3\text{He}$ or AFT data), are better predicted by t-T paths that cool to surface temperatures during the Laramide, consistent with an “old” Canyon. This inconsistency, which mimics the overall controversy, is reconciled by optimizing cooling paths so they are most consistent with multiple thermochronometers from the same rocks and adjusting parameters to account for model uncertainties. We adjusted model parameters to account for uncertainty in the rate of radiation damage annealing during sedimentary burial in these apatites and thus possible changes in He retentivity. In the westernmost Grand Canyon, peak burial conditions (temperature and duration) during the Laramide were likely insufficient to fully anneal radiation damage that accumulated during prolonged, near-surface residence since the Proterozoic. The combined AFT, AHe, and $^4\text{He}/^3\text{He}$ analysis of a key sample from Separation Canyon can only be reconciled by a “young” Canyon, but thermochronologic uncertainties remain large for this geologic scenario. Additional new AFT (5 samples) and AHe (3 samples) data in several locations along the canyon corridor also support a “young” Canyon and suggest the possibility of variable mid-Tertiary thermal histories beneath north-retreating cliffs. We conclude that application of multiple thermochronometers from common rocks reconciles conflicting thermochronologic interpretations and is best explained by a “young” westernmost Grand Canyon.

Chapter 2: Formation of the Grand Staircase

Dutton’s (1882) “Great Denudation” involved the lateral erosion of Mesozoic strata northwards from the rim of Grand Canyon via cliff retreat. He described a “great stairway” of alternating benches of erodible strata and cliffs of resistant strata now known as the Grand Staircase. We analyze 52 samples from across the southwestern Colorado Plateau and use linear inverse modeling of apatite thermochronometric data in HeFTy to determine continuous thermal histories for each sample. Results from these histories were then passed through a MATLAB code to extract temperatures of the weighted mean paths every 5 Ma, combined with geologic constraints on dated paleosurfaces, and interpolated across the study area. These interpolations show reconstructed cooling patterns of the top contact of the Kaibab Limestone through time since 70 Ma and can be used to estimate the geometry and rates of lateral cliff retreat and resulting erosional volumetric loss through time. We find three main times of denudational cooling, each associated with major through-going river systems. The Laramide orogeny (70–50 Ma) and incision of Paleocene fluvial valleys is associated with 55,750 cubic kilometers of volume loss above the Kaibab datum.

The 35–15 Ma ignimbrite flare-up, initiation of Basin and Range extension, and incision of the East Kaibab paleocanyon is associated with 37,000 cubic kilometers of volume loss above the Kaibab datum. Post-6-Ma river integration of the Colorado River system through Grand Canyon and probable young uplift is driving ongoing deep incision and is associated with a minimum of 15,500 cubic kilometers of volume loss above the Kaibab datum, with at least 4,166 additional cubic kilometers of volume loss from the Grand Canyon alone. Cliff retreat rates are highly lithology dependent and range between 1.8 km/Ma for the Chocolate Cliffs, 2.4 km/Ma for the Jurassic (Vermillion) Cliffs, and 1.8 km/Ma for the Grey Cliffs. We conclude that three periods of accelerated denudation of the southwestern Colorado Plateau, most likely driven by epeirogenic uplift, represent punctuated periods of broad-scale cliff retreat that are coeval with evidence for significant fluvial systems. The Colorado Plateau region is thus a type example of epeirogenic controls on geomorphic re-shaping of plateau landscapes.

Chapter 3: Provenance and Pathways of the Music Mountain and Buck and Doe Paleorivers

Scattered remnants of “Rim Gravels” on the southern margin of the Colorado Plateau preserve a direct record of its fluvial and erosional history. Two paleoriver deposits containing well-described gravels occur on the far southwestern corner of the plateau, the Paleocene (55–50 Ma) Music Mountain Formation and the Oligocene-early Miocene (24–18 Ma) Buck and Doe Conglomerates (Young, 1999). Detrital zircon analysis can provide clues to potential sources and sinks of these deposits and more recently, high-precision detrital sanidine studies have been developed to tightly constrain the maximum depositional ages and provenance of Cenozoic deposits. In this study, we use a combination of new and published detrital zircon and detrital sanidine data to determine provenance and potential sinks of the Music Mountain Formation ($n = 1090$ U-Pb zircon ages and $n = 5$ detrital sanidine ages used for maximum depositional ages) and the Buck and Doe Conglomerates ($n = 1028$ U-Pb zircon ages and $n = 6$ detrital sanidine ages used for maximum depositional ages). In addition, we collected 4 samples ($n = 670$ U-Pb zircon ages) from formations in the Table Cliffs Basin (e.g. Markagunt and Paunsaugunt Plateau regions) to evaluate it as a potential sink for the Music Mountain Formation.

Detrital zircon age populations for the Music Mountain Formation are dominated by a 1691 Ma age peak with a smaller 1390 Ma peak and a small portion of Mesozoic ages. Grenville-aged grains (~ 1100 Ma) are conspicuously absent. This age distribution indicates that the Music Mountain fluvial system is sourced from the nearby Kingman uplift, where basement rocks of these ages occur. Comparison of this age distribution with coeval Laramide deposits from the Uinta Basin, San Juan Basin, and Table Cliffs Basin reveal that while none of these basins are ideal matches, connections with the Table Cliffs or Uinta Basins are unlikely. The San Juan Basin provides a potential match for age populations, particularly the significant ~ 1390 Ma age peak,

and thus is preferred as a hypothesized sink for the Music Mountain fluvial system. The maximum depositional age via both detrital sanidine and detrital zircon is ~ 73 Ma, several tens of million years older than the best age estimates of 50–60 Ma and provides little new information.

Detrital zircon age populations for the Buck and Doe Conglomerate are also dominated by peaks at ~ 1680 Ma and 1390 Ma, although the 1390 Ma peak is significantly stronger in comparison with the older Music Mountain Formation. There are very minor peaks of Mesozoic-aged zircons and a sharp peak at ~ 20 Ma sourced from local volcanism, although this is only present in two of the 6 samples. These age populations suggest continued unroofing of the Kingman uplift with increased contribution from the 1390 Ma Peacock Mountain Granite and reworking of the Music Mountain Formation. Contemporaneous deposits include the lower portion of the Brown’s Park Formation from northern Utah and the Rainbow Gardens Formation in the Lake Meade region of eastern Nevada, and a sample from the Table Cliffs Basin that unexpectedly yielded a population of ~ 20 Ma zircon U-Pb ages. Comparison of age spectra for these units with the Buck and Doe ages indicate that a relationship with the Rainbow Gardens or the Brown’s Park Formation are unlikely, but that there is a high likelihood of a connection with the “White Claron” sample from the Table Cliffs Basin. Maximum depositional ages from detrital sanidine for three samples from the Buck and Doe Conglomerate are 18.065 ± 0.017 Ma, 25.52 ± 0.10 Ma, and 30.2 ± 0.2 ; the youngest of these is slightly younger than the Peach Springs Tuff (18.78 ± 0.02 Ma), which caps the type section of the Buck and Doe Formation.

The erosional history of the southern Colorado Plateau has been a topic of scientific debate for over 150 years. Key conclusions include 1) both of these fluvial systems were sourced from the Kingman uplift to the south as shown by the 1390 Ma age population, 2) a potential connection is proposed between the Music Mountain Formation and the San Juan Basin, which is also based on this 1390 Ma population, and 3) we also propose a ca. 18 Ma connection between the westernmost Buck and Doe sample and the Miocene “White Claron” of the Table Cliffs Basin, indicating there was no paleo Grand Canyon at that time. The timing of these fluvial systems is consistent with the major periods of denudation found in Chapter 2 and these paleorivers provide potential pathways for the removal of this material.

TRIPLE OXYGEN ISOTOPE COMPOSITION OF CARBONATES

Wostbrock, Jordan A.G., Ph.D.

This dissertation presents a method of analyzing the triple oxygen isotope compositions of carbonates, presents an empirical calibration of the carbonate-water equilibrium fractionation line, presents a triple oxygen isotope equipped fluid-rock mixing model for carbonates to see through diagenesis, and applies all these findings to ancient carbonate samples. Using modern carbonates and associate water, the following equations are calculated to describe equilibrium triple oxygen isotope fractionation of carbonates:

$$1000\ln\alpha^{18}\text{O}_{\text{cc-wt}} = \frac{2.84(\pm 0.02) \times 10^6}{T^2} - 2.96(\pm 0.19) \quad (1),$$

$$\theta_{\text{cc-wt}} = \frac{-1.39(\pm 0.01)}{T} + 0.5305 \quad (2).$$

Using these fractionation equations provides an extremely useful tool to determine whether a carbonate sample is altered or preserves its original isotopic composition. In samples that are altered, a fluid-rock mixing model is used to see through the diagenesis. Applying these tools to ancient carbonate rocks shows that many samples thought to be pristine are altered and are confusing paleoenvironmental interpretations. This work shows that seawater temperature and isotopic composition is unchanged over the Phanerozoic, an important consideration when reconstructing paleoenvironments.

STRUCTURAL AND GEOCHRONOLOGIC CONSTRAINTS ON THE DURATION OF THE PICURIS OROGENY AND DEMISE OF AN OROGENIC PLATEAU, NORTHERN NM
Young, Daniel J., M.S.

Metasedimentary and igneous basement rocks in northern New Mexico record episodic pulses of tectonism during cratonic growth from 1.8 to 1.38 Ga. Continued challenges involve parsing the deformational features attributable to the Yavapai Orogeny (1.71–1.68 Ga), Mazatzal orogeny (1.66–1.60 Ga), and Picuris orogeny (1.5–1.38 Ga) in this region and understanding how older structures may have been overprinted and reactivated to explain the observed strain. This paper presents regional cross-sections of the 1.7 Ga Vadito, 1.68 to 1.50 Ga Hondo,

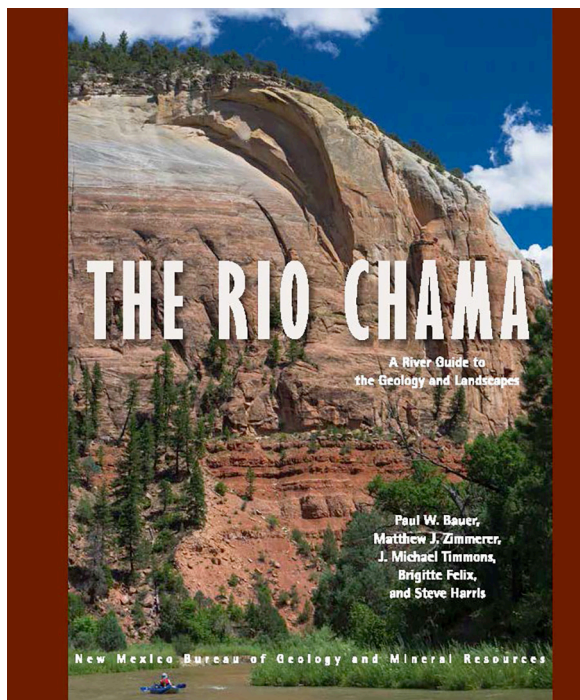
and 1.5–1.45 Ga Trampas groups of the Picuris Mountains and Rio Mora areas of northern New Mexico combined with new geochronologic and thermochronologic constraints. These data suggest the following tectonic evolution. An early bedding-parallel S1 fabric is present only in pre-Trampas Group rocks and is interpreted to be related to early isoclinal folds and thrusts. All groups were folded by F2 and F3 fold generations during the Picuris orogeny. New U-Pb dates from monazite cores of about 1.5 Ga in aluminous gneisses from the Vadito–Hondo group aluminous contact zone within the Pecos thrust sheet are interpreted as onset of Picuris orogeny prograde tectonism. This onset of heating/deformation is thus close in age, and apparently pre-dates deposition of the Trampas Group at 1488 ± 6 Ma in the footwall of the Pecos and Plomo thrusts. Growth of metamorphic garnets at 1.45–1.40 Ga from previous studies and new monazite rim dates of ~ 1.45 Ga may record metamorphism close in age to deposition of the thrust-bound 1.453 \pm 10 Ga Marqueñas Formation. Regional cross sections show that the modern surface exposure represents an exhumed ~ 15 km middle crustal duplex system that juxtaposes, from north to south: 1) 1.45 Ga triple point (>550 C, 3.5 kbars) polyphase metamorphic tectonites in the Copper Hill anticline–Hondo syncline thrust sheet made between the Pilar and Plomo thrusts, 2) a similar grade thrust-bound Marqueñas tectonite that makes up the Plomo shear zone, 3) the 1.45 Ga Peñasco granite that intrudes Vadito Group rocks between the Plomo shear zone and the Pecos master thrust, and 4) overriding volcanic rocks of the ~ 1.72 –1.65 Ga

Pecos volcanic complex. Juxtaposition of amphibolite-grade upper plate rocks against 1.48–1.45 Ga metasedimentary lower plate rocks are the product of progressive thrusting from 1.50 to 1.40 Ga, synchronous with development of syntectonic foreland basins. The 1.45 Ga granite and pegmatites show only minor penetrative strain but are considered broadly syntectonic with waning deformation at 1.45–1.40 Ga. A modern analog is the Tien Shan–Tarim basin region of the interior Tibetan Plateau inferred for the Picuris tectonism. New $^{40}\text{Ar}/^{39}\text{Ar}$ dates on hornblende and muscovite constrain cooling through $\sim 500^\circ\text{C}$ and ~ 350 – 400°C respectively and provide insight into cooling rates following the Picuris orogeny, and hence the nature and timing of demise of Picuris orogenic uplifts. Hondo and Trampas group rocks cooled through 500°C 1420–1381 Ma and through 350°C from 1378–1359 Ma. This is similar to new data with $^{40}\text{Ar}/^{39}\text{Ar}$ cooling data from muscovite from the Petaca pegmatite district (mean cooling age of 1375 ± 10 Ma), and similar ages in basement exposures from neighboring mountain ranges. Slow cooling from >500 to $<350^\circ\text{C}$ from ~ 1420 to ~ 1360 Ma suggests cooling rates of $\sim 3^\circ\text{C}/\text{Ma}$ over 60 Ma following peak triple point metamorphism. To explain this protracted cooling we propose that an orogenic plateau was built by thrust duplexing and penetrative folding in northern New Mexico during the Picuris orogeny followed by relatively slow erosional removal. Erosion of much of the region initiated by 1.1–1.3 Ga, resulting in deposition of the De Baca Group and correlative strata.

New Mexico Bureau of Geology and Mineral Resources Publications 2021

Upcoming Publication

The Rio Chama: A River Guide to the Geology and Landscapes



The 135-mile Rio Chama of northern New Mexico is a major tributary of the Rio Grande. From its alpine headwaters at the Continental Divide of the glaciated San Juan Mountains in southern Colorado, this hidden gem flows across the Colorado Plateau in a spectacular canyon cut into Mesozoic sedimentary rocks, in places up to 1,500 feet deep. Towering, vibrant, sandstone cliffs, heavily wooded side canyons, superb camping, and a diversity of historical sites offer an outstanding wild river backdrop for the boater, angler, hiker, or camper.

This book contains detailed river maps of the seven sections of the Rio Chama, plus its three resplendent reservoirs, from the Colorado headwaters to its confluence with the Rio Grande near Española. The Chama Canyon section, below El Vado Dam and through the Chama Canyon Wilderness, is one of the finest, multi-day, whitewater trips in the Southwest. The Rio Chama will be printed in 2021.

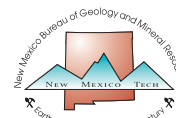
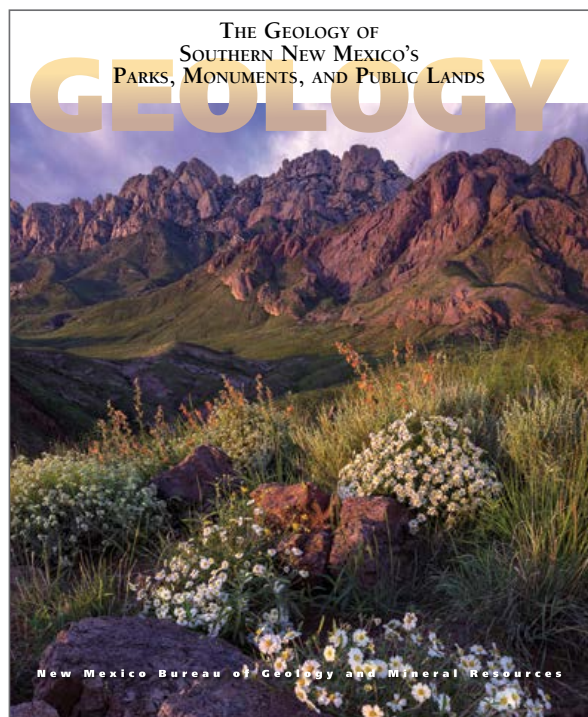
Available at our bookstore!

Order online or call 575-835-5490!

*The Geology of Southern New Mexico's Parks, Monuments, and Public Lands is the companion book to **The Geology of Northern New Mexico's Parks, Monuments, and Public Lands.***

Available Now!

Mount Taylor map and guide book!



For more information about the bureau, our publications or to order online, visit our website at geoinfo.nmt.edu.

Call (575) 835-5490 or email us at

NMBG-Publications@nmt.edu

New Mexico Tech

801 Leroy Place, Socorro, New Mexico 87801

